# Temporal Variability in Gas Emissions at Bagana Volcano Revealed by Aerial, Ground, and Satellite Observations

Brendan McCormick Kilbride[1], Emma J Liu[2], Kieran T Wood[3], Thomas C Wilkes[4], C Ian Schipper[5], Kila Mulina[6], Ima Itikarai[7], Thomas S Richardson[8], Cynthia Werner[9], Catherine SL Hayer[3], Benjamin Esse[1], Mike Burton[1], Tom D. Pering[4], Andrew J. S. McGonigle[4], Diego Coppola[10], Marcello Bitetto[11], Gaetano Giudice[12], and Alessandro Aiuppa[13]

[1]University of Manchester
[2]Department of Earth Sciences, University College London
[3]The University of Manchester
[4]University of Sheffield
[5]Victoria University of Wellington
[6]rabaul volcano observatory
[7]Rabaul Volcano Observatory
[8]University of Bristol
[9]Cascades Volcano Observatory, United States Geological Survey
[10]Università di Torino
[11]University of Palermo
[12]Istituto Nazionale di Geofisica e Vulcanologia
[13]Università di Palermo

December 7, 2022



## Abstract

Bagana is a remote, highly active volcano, located on Bougainville Island in southeastern Papua New Guinea. The volcano has exhibited sustained and prodigious sulfur dioxide gas emissions in recent decades, accompanied by frequent episodes of lava extrusion. The remote location of Bagana and its persistent activity have made it a valuable case study for satellite observations of active volcanism. This remoteness has also left many features of Bagana relatively unexplored. Here, we present the first measurements of volcanic gas composition, achieved by unoccupied aerial system (UAS) flights through the volcano's summit plume, and a payload comprising a miniaturised MultiGAS. We combine our measurements of molar $CO_2/SO_2$ ratio in the plume with coincident remote sensing measurements (ground- and satellite-based) of $SO_2$ emission rate, to compute the first estimate of $CO_2$ flux at Bagana. We report low $SO_2$ and $CO_2$ fluxes at Bagana from our fieldwork in September 2019, ˜320 ± 76 $td^{-1}$ and ˜320 ± 84 $td^{-1}$ respectively, which we attribute to the volcano's low level of activity at the time of our visit. We use satellite observations to demonstrate that Bagana's activity and emissions behaviour are highly variable and advance the argument that such variability is likely an inherent feature of many volcanoes worldwide and as yet is inadequately captured by our extant volcanic gas inventories, which are often biased to sporadic measurements. We argue that there is great value in the use of UAS combined with MultiGAS-type instruments for remote monitoring of gas emissions from other inaccessible volcanoes.

## Hosted file

`bagana-drone-manuscript_btmk-nov22_submission_supplementarymaterial.docx` available at

https://authorea.com/users/563915/articles/610986-temporal-variability-in-gas-emissions-at-bagana-volcano-revealed-by-aerial-ground-and-satellite-observations

# Temporal Variability in Gas Emissions at Bagana Volcano Revealed by Aerial, Ground, and Satellite Observations

**B. T. McCormick Kilbride[1,2], E. J Liu[3], K. T. Wood[4], T. C. Wilkes[5], C. I. Schipper[6], K. Mulina[7], I. Itikarai[7], T. Richardson[8], C. Werner[9], C. S. L. Hayer[1], B. Esse[1], M. Burton[1], T. D. Pering[5], A. J. S. McGonigle[5], D. Coppola[10], M. Bitetto[11], G. Giudice[11], A. Aiuppa[11]**

[1]Department of Earth and Environmental Sciences, The University of Manchester, UK
[2]Centre for Crisis Studies and Mitigation, The University of Manchester, UK
[3]Department of Earth Sciences, University College London, UK
[4]Department of Mechanical, Aerospace & Civil Engineering, The University of Manchester, UK
[5]Department of Geography, University of Sheffield, UK
[6]Department of Earth Sciences, Victoria University of Wellington, NZ
[7]Rabaul Volcanological Observatory, PNG
[8]Department of Aerospace Engineering, University of Bristol, UK
[9]U.S. Geological Survey (contractor), New Plymouth, NZ
[10]Dipartimento di Scienze della Terra, Università di Torino, Italy
[11]Dipartimento di Scienze della Terra e del Mare, Universit à di Palermo, Italy

Corresponding author: Brendan T. McCormick Kilbride
(brendan.mccormickkilbride@manchester.ac.uk)

**Key Points:**

- We present the first measurements of volcanic gas composition at Bagana volcano.
- $CO_2$ and $SO_2$ fluxes at Bagana vary widely with levels of unrest, from ~$10^2$-~$10^4$ $td^{-1}$
- Unoccupied aerial systems (drones) are of great value in monitoring emissions from inaccessible volcanic summits.

## Abstract

Bagana is a remote, highly active volcano, located on Bougainville Island in southeastern Papua New Guinea. The volcano has exhibited sustained and prodigious sulfur dioxide gas emissions in recent decades, accompanied by frequent episodes of lava extrusion. The remote location of Bagana and its persistent activity have made it a valuable case study for satellite observations of active volcanism. This remoteness has also left many features of Bagana relatively unexplored. Here, we present the first measurements of volcanic gas composition, achieved by unoccupied aerial system (UAS) flights through the volcano's summit plume, and a payload comprising a miniaturised MultiGAS. We combine our measurements of molar $CO_2/SO_2$ ratio in the plume with coincident remote sensing measurements (ground- and satellite-based) of $SO_2$ emission rate, to compute the first estimate of $CO_2$ flux at Bagana. We report low $SO_2$ and $CO_2$ fluxes at Bagana from our fieldwork in September 2019, ~320 ± 76 $td^{-1}$ and ~320 ± 84 $td^{-1}$ respectively, which we attribute to the volcano's low level of activity at the time of our visit. We use satellite observations to demonstrate that Bagana's activity and emissions behaviour are highly variable and advance the argument that such variability is likely an inherent feature of many volcanoes worldwide and as yet is inadequately captured by our extant volcanic gas inventories, which are often biased to sporadic measurements. We argue that there is great value in the use of UAS combined with MultiGAS-type instruments for remote monitoring of gas emissions from other inaccessible volcanoes.



## Plain Language Summary

Bagana is a remote and highly active volcano in southeastern Papua New Guinea. Historically, it has been among the most active volcanoes in PNG, notable for its long-lived eruptions and sustained gas emissions. Bagana has only been infrequently studied before now. We used unoccupied aerial systems (drones) along with ground- and satellite-based remote sensing data to characterise the chemical composition and flux of Bagana's gas emissions and place these in the context of global volcanic emissions. Owing to low activity during the time of our fieldwork, we report lower than anticipated emissions of carbon dioxide and sulfur dioxide from Bagana. We argue that characterizing highly variable volcanic emissions is challenging without long-term continuous observations and that, for remote volcanoes like Bagana, both drones and satellite observations are powerful tools to undertake these observations.

## 1 Introduction

Bagana volcano, located on Bougainville Island in southeastern Papua New Guinea (6.137 °S, 155.196 °E; 1855 m a.s.l.), is among the most active volcanoes on Earth with a record of semi-continuous lava extrusion stretching back to at least the mid-nineteenth century (Bultitude, 1976). Bagana may also be one of the youngest of Earth's active volcanoes; recent estimates suggest the modern edifice may have grown in only 300-500 years (Wadge et al., 2018). Satellite observations over the past two decades indicate that Bagana is a prodigious source of sulfur dioxide ($SO_2$) gas into the atmosphere, with a mean annual emission rate of 1379 ± 89 kt $yr^{-1}$ during 2005-15 (Carn et al., 2017). Bagana has been predicted to be a major emitter of volcanic carbon into the atmosphere (~6245 t $d^{-1}$), based on global correlations between whole-rock Ba/La ratios and volcanic gas plume $CO_2/S_T$ ratios (Aiuppa et al., 2019; Werner et al., 2019), but the chemical composition of Bagana's gas emissions has never before been measured directly.

The Bagana edifice is steep and unstable, and prone to rockfalls and debris avalanches (Bultitude, 1976). The volcano cannot be climbed safely to deploy gas sensors directly in the plume (c.f. Aiuppa et al., 2005; de Moor et al., 2017). Recently, unoccupied aerial systems (UAS, or drones) have been used by volcanologists seeking to measure or sample gas emissions from remote or hazardous summits (McGonigle et al., 2008; Rudiger et al., 2018; Stix et al., 2018; Liu et al., 2019; Kazahaya et al., 2019; James et al., 2020; Pering et al., 2020; Liu et al., 2020a). Herein, we present the first measurements of volcanic gas chemistry at Bagana, achieved by flying a miniaturized gas sensing payload through Bagana's summit gas plume on-board a UAS. We also present simultaneously acquired remote sensing measurements of $SO_2$ emission rate. We calculate $CO_2$ emission rates by multiplying MultiGAS-measured $CO_2/SO_2$ ratios by these $SO_2$ emission rates (de Moor et al., 2017; Werner et al., 2019).

Bagana's $SO_2$ emissions during our fieldwork (13-20 September 2019) were lower than the emission rates calculated from satellite observations in 2005-17 (McCormick Kilbride et al., 2019). Consequently, our calculated $CO_2$ emission rates for Bagana are rather lower than those predicted (Aiuppa et al., 2019). We evaluate these results in the context of changeable levels of activity at Bagana, as evidenced by multi-year satellite-based TROPOMI measurements of $SO_2$ emissions, and the possibility of shallow (i.e. hydrothermal) influences on volcanic gas emissions.

Our results support the developing paradigm that many, and perhaps most, of Earth's volcanoes exhibit wide variations in their gas emissions through time, which can hamper our ability to build volcanic emissions inventories based on short-duration field campaigns or assumptions regarding characteristic activity informed by historical trends (McCormick et al., 2015; de Moor et al., 2017; Werner et al.ure, 2019). Remote volcanoes such as Bagana pose a challenge for the establishment of conventional monitoring networks, and therefore both UAS- and satellite-based methods will be valuable tools for characterising emissions in such settings.

## 2 Data and Methods

The key methods used in this study are remote sensing measurements (ground-based UV camera, UAS- and boat-based DOAS spectrometer traverses, satellite-based UV spectroscopy) of $SO_2$ flux and UAS-enabled in-plume measurements of volcanic gas composition ($CO_2/SO_2$ molar ratio), using a MultiGAS sensor. $CO_2$ flux is computed from the product of $SO_2$ flux and $CO_2/SO_2$ mass ratio.

### 2.1 Geological Context

Bagana is one of seventeen post-Miocene volcanoes on Bougainville Island (Figure 1; Blake, 1968). This volcanism is a consequence of plate convergence, with the Solomon Sea plate being subducted to the northeast beneath the Pacific plate (Holm et al., 2016). Bagana is a stratovolcano of basaltic andesite composition, sometimes described as a "lava cone", being constructed largely of overlapping lava flows with relatively little pyroclastic material (Bultitude et al., 1978). The lava flows are rubbly with prominent marginal levees and steep fronts strewn with talus and fallen boulders. Block-and-ash flows and lahar deposits cover much of the lower northwestern slopes.

Bagana's characteristic activity comprises the alternation of extrusive eruptions persisting for several months and quiescent intervals dominated by voluminous passive degassing. Comprehensive reviews of Bagana's activity are provided by Bultitude (1976), Bultitude et al. (1978, 1981, 1981a) and, more recently, by Wadge et al. (2018) and McCormick Kilbride et al. (2019). The volume of the Bagana edifice is estimated to be 5.1-9.6 $km^3$, depending on the (unknown) geometry of the underlying topography (Wadge et al., 2018). If the mean extrusion rate of 1.0 $m^3\ s^{-1}$ calculated over the last 70 years is representative, the edifice may have been built in only 300-500 years. Intriguingly, the neighbouring pyroclastic shield volcano, Billy Mitchell, experienced a caldera-forming VEI 6 eruption 370 ± 19 years before present. Wadge et al. (2018) speculated that there may be a genetic link between caldera collapse and the cessation of activity at Billy Mitchell and the onset of lava extrusion and edifice construction at Bagana.

Measurements of Bagana's gas emissions consistently place it among the largest global volcanic $SO_2$ sources. Two recent studies used observations from the satellite-based Ozone Monitoring Instrument (OMI). Carn et al. (2017) reported a mean SO2 flux of 1380 kt $yr^{-1}$ (3780 t $d^{-1}$) in 2005-15. McCormick Kilbride et al. (2019) distinguished mean co-extrusive and quiescent $SO_2$ emission rates of 3300 t $d^{-1}$ and 2500 t $d^{-1}$ respectively, in 2005-17. Ground-based and airborne UV remote sensing measurements in the 1980s and 2000s found $SO_2$ emissions in the range of 2000-3200 t $d^{-1}$ (McGonigle et al., 2004; Andres and Kasgnoc, 1998). While no measurements have been made of $CO_2$ emissions from Bagana, Aiuppa et al. (2019) predicted a flux of 6245 ± 2335 $td^{-1}$, based on the combination of Carn et al. (2017)'s reported $SO_2$ flux and an assumed $CO_2/S_T$ of 2.4 ± 0.7. The latter ratio is based on global correlations between whole-rock Ba/La and volcanic gas plume $CO_2/S_T$, with Bagana posited by Aiuppa et al. (2019) to be a moderately carbon-rich system, with the local mantle wedge volatile budget being augmented by carbon released from sedimentary lithologies on the nearby subducting slab.

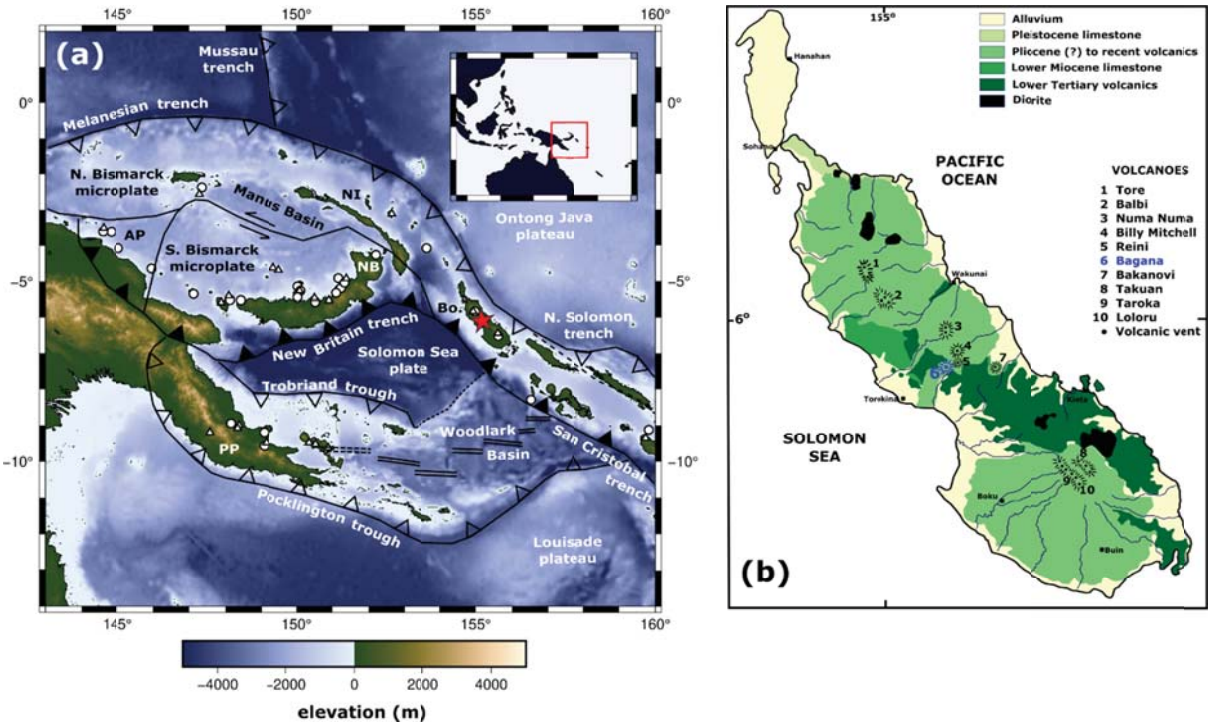


**Figure 1.** Left panel shows regional geology with key tectonic features marked, after Holm et al. (2016). Bagana is marked with the red star. AP = Adelbert Plate, NB = New Britain, NI = New Ireland, Bo. = Bougainville; PP = Papuan Peninsula. Active plate convergence is marked by black filled triangles; inactive convergent margins are indicated by open triangles. Topography and bathymetry is from the ETOPO1 Global Relief Model (https://www.ngdc.noaa.gov/mgg/global/global.html). Right panel shows Bougainville geological map, with major lithologies and volcanic edifices after Blake (1968).

Bagana erupts porphyritic basaltic andesite lavas with a phenocryst assemblage of augite, plagioclase and amphibole and a mean whole-rock $SiO_2$ content of 55.5 ± 1.5 wt. % (Bultitude et al., 1978). The volume of lava erupted over the last decade appears to be insufficient to supply all the gas emitted over the same interval, unless the melt sulfur concentration exceeds ~5000 ppm, or alternatively the prodigious emissions are sourced from a deeper, non-erupted magma (McCormick Kilbride et al., 2019, Edmonds et al., 2022). At present, there are no petrological or geochemical data to place constraint on the volatile content of the magmas feeding Bagana's eruptions.

## 2.2 UAS Gas Composition Flights

*Titan.* Our principal UAS is a fixed-wing aircraft, custom-built at the University of Bristol and based on the twin-propeller V-tail 'Titan' airframe from Skywalker (China). The Titan has a take-off weight of 8.5 kg (including 1.0 kg payload) and a wingspan of 2.1 m. The aircraft is powered by a 12.7 Ah 6S 22.2 Lithium Polymer (LiPo) battery, can be hand-launched, and lands with the assistance of a parachute (Figure 3). We demonstrated effective use of the Titan on two previous expeditions to Papua New Guinea, making the first measurements of gas composition at Manam volcano (Liu et al., 2020a; Wood et al., 2020). Bagana represents a comparable target in terms of the required endurance (20-25 minute flights, with gas sensing measurements undertaken around 2000 m above take-off altitude and up to 7 km horizontal distance from take-off location).

The Titan is equipped with a full auto-pilot computer and supporting sensors (GNSS, barometric altitude, airspeed indicator, and inertial measurement unit). During flight, we interact with the aircraft via three wireless links: a pilot safety link (433 MHz), a bi-directional telemetry modem (868 MHz) and a first person view (FPV) video stream (2.4 GHz). The pilot safety link is used to toggle between automated flight paths and intervals of semi-manual control (Fly-By-Wire mode). The bi-directional modem allows us to monitor flight statistics (e.g. battery consumption) and real-time gas concentrations from the onboard sensor payload, and to pass new commands to the autopilot. The FPV link aids our ground team in adjusting the aircraft during manual flight intervals, for example, by directing passage through notably thick portions of the volcanic gas plume.

We launched and recovered the Titan from the hamlet of Tsihokoa (6.159° S, 155.137° E, 150 m a.s.l.) in the Wakovi community, a small ridge above the Torokina river to the west of Bagana (Figure 2). We selected this site because it afforded a clear view of the volcano and plume, had a large open field available for our landing site, and enabled straightforward hand launch of the aircraft into the prevailing wind. To intercept the Bagana plume, we programmed automated flight paths with an altitude gain of 1700-2000 m and horizontal traverses of 7 km. We obtained permission for these beyond visual line of sight (BVLOS) flight operations from the Civil Aviation Safety Authority of Papua New Guinea. Our pre-programmed flight paths (example in Figure 2, full series available as a .kml file in Supplementary Material) comprised a sequence of waypoints between take-off,a zig-zag ascent path (with optimised ascent rate, climb angle, airspeed etc chosen based on our experience from previous campaigns), gas sensing over the volcanic summit, a glide back to the recovery area, and a loiter pattern for the aircraft to maintain until we could safely execute a manual landing. We developed our flight paths iteratively, combining a high-resolution topography model with our own observations of the volcanic summit and plume, both from the ground and from the FPV video stream. We made in-flight adjustments (switching to Fly-By-Wire mode) where necessary, based on real-time readouts from the on-board $SO_2$ gas sensor. This capability is valuable in that it allows a pilot to change mission targets during flight and also respond quickly to in-flight hazards.

*MultiGAS.* The Titan carries a miniaturised MultiGAS sensor package, built at the University of Palermo, in a fuselage payload bay (Aiuppa et al., 2007; Liu et al., 2018; Pering et al., 2020; Liu et al., 2020). The instrument samples ambient air or volcanic gases through an inlet tube outside the fuselage, connected to a pump capable of a 10 L/min flow rate. The gas passes through a 1-

μm particle filter before reaching the sensors. Data are logged at 1 Hz, to an on-board micro-SD card and by telemetry to the ground station. The MultiGAS is equipped with $SO_2$ and $H_2S$ electrochemical sensors (City Technology T3ST/F-TD2G-1A and T3H-TC4E-1A, respectively), calibrated for 0-200 and 0-50 ppmv, respectively, with accuracy of ± 2% and resolution of 0.1 ppmv. There is a 13% $SO_2$ cross-sensitivity on the $H_2S$ sensors and, as described below, we did not detect $H_2S$ in the Bagana plume. We measure $CO_2$ concentration with a non-dispersive infrared spectrometer (Microsensorik Smartgas Modul Premium2), calibrated for 0-5000 ppmv with accuracy of ± 2% and resolution of 1 ppmv. To avoid radio interference from the UAS transmission system, we wrap the $CO_2$ spectrometer in brass foil, and then encase the whole sensor payload in a foil bag. We calibrated the sensors with standard reference gases at the University of Palermo before the expedition and again afterwards, and found no evidence for sensor drift. We can calculate $H_2O$ concentration from measurements of pressure (± 1 hPa), temperature (± 0.5 °C), and humidity (± 3 %) with an on-board Bluedot BME280 sensor. The Bluedot failed on our second flight due to exposure to liquid water (rain) in the plume; our backup sensor malfunctioned on the following flight. Therefore, we lack humidity, pressure, and temperature data for the majority of our flights, precluding calculation of $H_2O$ concentration.

Each flight yields a time series of gas concentration for each sensor, which we post-processed using MATLAB® and Ratiocalc software (Tamburello, 2015). $CO_2$ concentrations were internally compensated for temperature (± 0.2% full span per °C). We did not make any barometric pressure correction in the calculation of $CO_2$ concentration: our gas ratios are derived from relative changes in concentration and we flew the UAS at constant altitude during the plume interceptions (Flights 4-6) for which we present data. We distinguish volcanogenic (or 'excess') $CO_2$ from atmospheric background, which we define as the mean $CO_2$ concentration measured during constant altitude flight in $SO_2$-free air, updating the value for each flight. We measured no $H_2S$ concentrations exceeding the 13% cross-sensitivity of the sensor to $SO_2$ (determined during calibration with standard reference gases), and we therefore consider $H_2S$ undetected in the Bagana plume.

We account for different sensor response characteristics within the MultiGAS array by applying a Lucy-Richardson deconvolution algorithm to the $CO_2$ time series (Wood et al., 2019; Liu et al., 2020a; Pering et al., 20020). The algorithm is initiated using the measured time series and makes use of a sensor model determined empirically from the response of the NDIR to step changes in calibration gas concentration. The sensor model is best described by a windowed integral and is essentially an N-point moving average applied to the 'true' input signal: laboratory tests conducted by Wood et al. (2019) identified the $CO_2$ sensor to average over approximately 15 seconds, hence N=15. The deconvolution effectively removes the sensor's inherent filtering effect and the processed $CO_2$ concentration time series shows concentration peaks (i.e. plume intercepts) that are steeper, narrower and marginally greater in amplitude than the measured signal, without changing the integrated area beneath the peak. We calculate $CO_2/SO_2$ ratios by fitting linear regressions to scatterplots of $SO_2$ concentration and our deconvolved $CO_2$ concentrations. The data selected for inclusion in each fitting are those measured by each sensor during 'plume intercepts', intervals where both $SO_2$ and $CO_2$ sensors record coincident concentration peaks as the UAS passes into, through, and beyond the volcanic gas plume. The horizontal speed of the Titan is ~20 $ms^{-1}$ and the duration of our plume intercepts range from ~30-70 seconds.

251

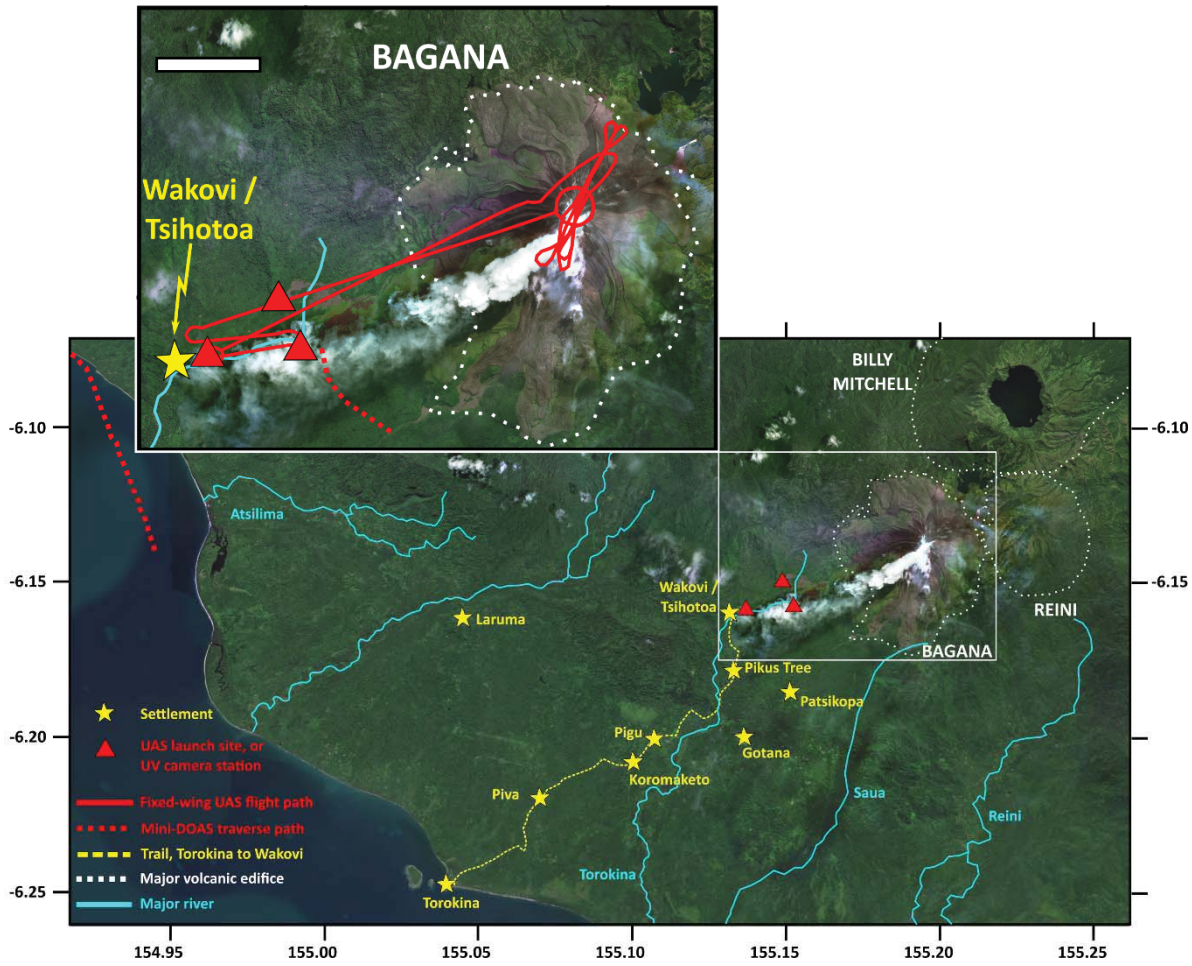


**Figure 2**. Satellite image (courtesy Bing Imagery) of Bagana surroundings with key locations from our fieldwork identified. We have omitted the flight paths shown in the inset from the main panel for clarity. Adjacent to Bagana are two dormant volcanoes, the pyroclastic shield Billy Mitchell with its summit crater lake and the deeply incised edifice Reini, probably of Pleistocene age. The representative fixed-wing UAS flight path shown corresponds to Flight 6. Paruata Island (Figure 5) is visible offshore from Torokina. Note that the plume shown here is characteristic of Bagana's emissions, which disperse generally towards the southwest, but this image was not acquired during our work in September 2019.


**Figure 3**. (a) Hand launch of the Titan aircraft, facing into slight wind and from an elevated position on a ridge at 6.159° S, 155.137° E. (b) Parachute landing of the aircraft in a field adjacent to the take-off site.

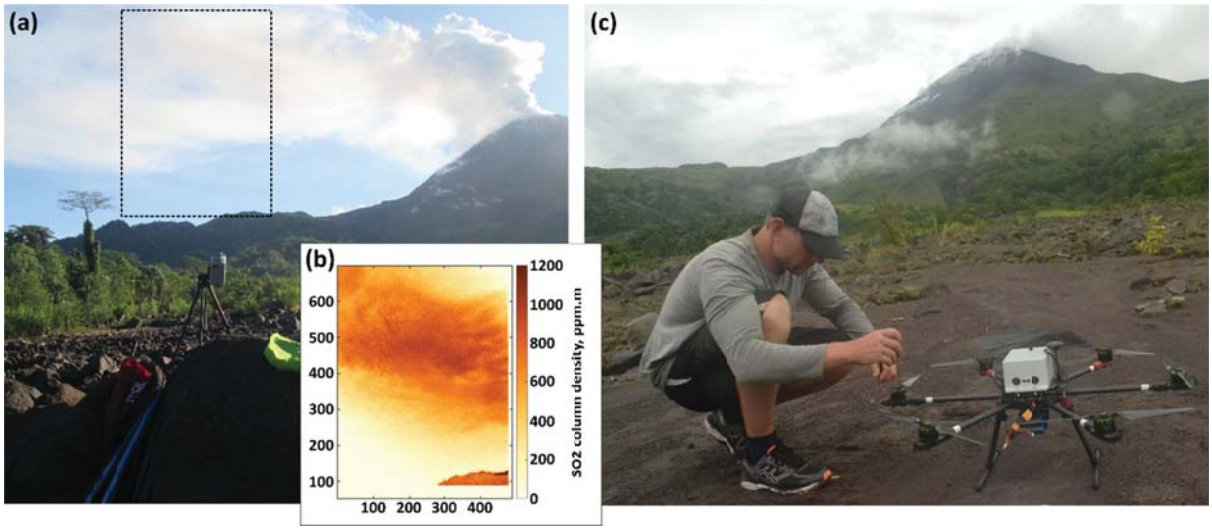


**Figure 4**. (a) View of Bagana and its gas plume from the UV measurement location (-6.158 °S, 155.152 °E). Distance to volcano is around 4 km. Dashed box indicates the approximate field of view of the camera while acquiring data. (b) Representative absorption image, with darker colours indicating higher $SO_2$ column density. Ticks and labels on the left and lower edges of the images indicate the scale of the field of view, recorded in metres. (c) Crabcopter pre-flight checks. The miniDOAS spectrometer is housed in the grey box mounted on the upper surface of the UAS.

### 2.3 Ground-, UAS-, and Satellite-Based Remote Sensing

We measured $SO_2$ emission rates in the field using ultraviolet (UV) spectroscopy, with (1) zenith-pointing spectrometers (e.g. Galle et al., 2003; Kern et al., 2012) making traverses beneath the plume and (2) PiCam UV cameras (Wilkes et al., 2016, 2017). Following the field campaign, we studied $SO_2$ emissions from Bagana over longer intervals using the satellite-based spectrometer TROPOMI (Theys et al., 2019; Queisser et al., 2019, Burton et al., 2021).

*Spectrometer traverse measurements.* We made traverses by mounting spectrometers on both a second UAS and a boat. This UAS (the 'Crabcopter', Figure 4) is a multirotor aircraft under development at the Victoria University of Wellington. This expedition was the first field deployment of the aircraft, which is controlled via wireless link. The operator can view the progress of the aircraft in-flight via a video feed from the on-board action camera, telemetered to a tablet mounted on the ground control unit.

We flew exclusively manual (c.f. automated, pre-programmed) flights with the Crabcopter, aiming to make lateral traverses beneath the plume, flying at a steady altitude of 500 m above the ground, from a launch and recovery site at -6.158 °S, 155.152 °E, around 4 km from the volcano's summit. We were restricted to short observation windows (<1 hour) by persistent cloud cover and achieving a full traverse (i.e. passing from clean air, beneath the plume, and back to clean air) proved challenging due to the large width of the plume (>5 km). During our interval of best (clear-sky) measurement conditions, gas seemed to be ponding around the upper slopes of the edifice, making for large effective plume widths that came close to exceeding the Crabcopter's endurance. Our best traverse, on 17 September, was incomplete and to calculate an emission rate from this measurement we have had to make an assumption of plume symmetry.

We made further measurements by spectrometer while leaving the field area by boat on 20$^{th}$ September. We passed beneath Bagana's downwind plume to the southwest (30-40 km from summit, Figure 2); the plume was visible extending a great distance out to sea to our west. At this distance, the plume width was roughly 15 km.

The spectrometer payload is a miniature ultraviolet differential optical absorption spectrometer, or miniDOAS. The instrument quantifies the slant column concentration of a trace gas, here $SO_2$, in its field of view, using scattered sunlight as a light source. The change in light intensity along a known path length due to absorption by $SO_2$, relative to a blue-sky spectrum free of $SO_2$, can be related directly to the $SO_2$ column concentration. Spectral data were acquired between 280 and 500 nm at 0.6 nm resolution and at approximately 1 Hz using an Ocean Optics FLAME-S spectrometer, and the instrument position was tracked using a Ublox NEO-6M GPS receiver. From the vertical column densities we obtain in each plume traverse, we can calculate an integrated plume cross section of $SO_2$ concentration. Multiplication of this integrated section by the plume's speed (either from meteorological observations or a model value) provides us with an estimate of $SO_2$ emission rate. Here, we use wind data from *GDAS, which is the National Center for Environmental Prediction (NCEP) Global Data Assimilation System (https://www.ncdc.noaa.gov/data-access/model-data/model-datasets/global-data-assimilation-system-gdas)*. The emission rate error is determined by propagating the errors of the input parameters $SO_2$ column density, wind speed and wind direction by assuming that the individual

errors are independent of another. The error in the $SO_2$ column density is determined from the quality of the spectral fit.

*UV camera measurements.* The PiCam is a low-cost $SO_2$ (UV) camera, built around two modified Raspberry Pi camera modules (Wilkes et al. 2016, 2017). The modules (Omnivision OV5647) are modified by chemical removal of the sensor's Bayer filter, which increases the detector's responsivity to UV radiation and removes the mosaic patter response imposed by the Bayer filter (Wilkes et al., 2016). The optical system for the PiCam is built from a 3D printed lens holder and an off-the-shelf plano-convex lens (9 mm focal length, 6 mm diameter; Edmund Optics Inc.) with a resulting field-of-view of 23.1˚ × 17.3˚ (width × height). Each camera module is equipped with a bandpass filter (Edmund Optics Inc.), one centred at 310 nm and the second at 330 nm (each with 10 nm bandpass full-width-at-half-maximum), which are, respectively, typical on- and off-bands for the detection of $SO_2$ (Mori and Burton, 2006). The cameras are connected to Raspberry Pi 3 Model B computers for interfacing and are housed, along with batteries and a GPS unit, in a Pelicase. We control the PiCam from a Windows laptop via wireless link and manage data capture via custom Python 3 code (Wilkes et al., 2016, 2017).

We carried out image processing after acquisition, not in real-time, and again using custom Python 3 code. Gliss et al. (2017) have reviewed $SO_2$ camera image processing techniques in detail; we primarily use the protocols outlined by Kantzas et al. (2010). Our images are all dark image corrected and we correct for vignetting using a clear-sky mask acquired in the field. To assess clear-sky background intensity we measure the average intensity of light in a region of sky close to the plume without volcanic gas. We calibrated our apparent absorbance images using three gas cells of known $SO_2$ column densities (0, 412 and 1613 ppm.m). The column densities we measured during the field campaign were all within this calibration range, therefore we were not required to extrapolate to higher values. We extracted integrated column amounts from a line perpendicular to plume transport (Figure 4) and calculated plume speed with the cross-correlation technique (Mori and Burton, 2006). The prevailing environmental conditions were extremely challenging for UV spectroscopy, with high atmospheric water vapour, persistent cloud cover throughout each day from around 0900 onwards and relatively low UV levels during the early morning and late afternoon clear-sky intervals. Our period of best quality acquisition comprised around one hour on the morning of 18 September.

Assuming a 10% uncertainty in our estimated distance from the PiCam to the plume, the estimated distance between integrated column lines for cross-correlation has a corresponding uncertainty of 10%. This translates to a 10% uncertainty in wind speed estimation. We calculated the integrated column amount uncertainty using the PiCam's detection limit of the system, estimated as 180 ppm.m following the method of Kern et al. (2010). Using this as the $SO_2$ column amount uncertainty and summing in quadrature across each pixel of the integrated column gives an overall integrated column uncertainty (Wilkes et al., 2017). Light dilution for the plume, given a distance of around 3 km is likely to be below 20% (estimated after Campion et al., 2015), although we are unable to confirm this and we consider 20% to be a conservative estimate. We estimate the cell calibration uncertainty to be 10%, following the manufacturer quoted uncertainty of the gas cell column amounts. Summing all uncertainties in quadrature, our SO2 camera data are subject to a total uncertainty of 0.7-1.2 $kgs^{-1}$, or ≈25% (Figure 9a).

*Satellite observations.* The Tropospheric Monitoring Instrument, TROPOMI, is a hyperspectral imaging spectrometer carried by the European Space Agency (ESA)'s Sentinel-5 Precursor (S-5P) satellite (Veefkind et al., 2012). Launched in 2017 and operational since April 2018, TROPOMI had a spatial resolution of 7 × 3.5 $km^2$ (thirteen times better than the earlier Ozone Monitoring Instrument, OMI), which was improved to 5.5 × 3.5 $km^2$ in August 2019. This fine spatial resolution has enabled the mapping of atmospheric $SO_2$ concentrations with unprecedented detail, in turn enabling the most comprehensive overview yet of volcanic outgassing as observed from space, including monitoring of $SO_2$ emission rates in both syn- and inter-eruptive episodes at sub-daily temporal resolution (Theys et al., 2019; Queißer et al., 2019).

In this study we use the COBRA (Covariance-Based Retrieval Algorithm) Level 2 $SO_2$ TROPOMI dataset (https://distributions.aeronomie.be, accessed Feb. 2022; Theys et al., 2021). We calculated $SO_2$ emission rates from TROPOMI using the PlumeTraj analysis toolkit (Queißer et al., 2019; Burton et al., 2020). The toolkit, written in Python 3, uses the HYSPLIT trajectory model (Draxler & Hess, 1998), to calculate backward trajectories for all pixels in the satellite field of view with confirmed detection of volcanic $SO_2$. Wind shear within the atmosphere causes trajectories at different altitudes to move at varying speeds and directions; thus we can isolatie those that intersect with the source volcano.

To remove noise from our quantification of $SO_2$ emission rates, we perform two initial thresholding tests on each pixel: 1) the $SO_2$ concentration must exceed three times the random noise for that pixel; 2) two of the surrounding eight pixels must also pass this test, removing spurious high concentration pixels. We run all pixels that pass these thresholding tests through the PlumeTraj trajectory analysis. We assign the trajectory that passes closest to the volcano as the optimal trajectory for that pixel, discarding the pixel if the approach distance exceeds 250 km. This optimal trajectory gives us the altitude at the time of measurement, the injection altitude, and the injection time. Since the $SO_2$ vertical column density (VCD, i.e. concentration) is dependent upon the plume's altitude, raw TROPOMI data are provided assuming three altitudes (1, 7, and 15 km). We use a linear interpolation between these prescribed altitudes to obtain a corrected concentration for each pixel. We multiply this concentration by the pixel area to give the $SO_2$ mass which, when combined with the injection time and performed for all pixels in the plume, yields an emission flux time series. We can then average this flux time series to give a daily emission rate, which is reported within this study, along with the peak 1-hour emission rate for each day.

In addition to our PlumeTraj analysis, we calculate monthly mean emission rates (expressed as $td^{-1}$ for each month of the study interval) by regridding and averaging the 1 km COBRA TROPOMI data. Our method follows Theys et al. (2021), using only high-quality pixels (i.e. we discard the outermost 25 pixels from both edges of the swath, those with a cloud fraction >30%, or those with a solar zenith angle >60°) and performing spatial averaging using a 10-point box car average. We stack the regridded data and then divide by the number of positive detections within each grid box. We perform the mass calculation for a 4° box centred on Bagana, with the averaged VCD from each grid box multiplied by its area and then summed. This approach also provides maps of monthly mean $SO_2$ VCD over the study region (Figure 11, Supplementary Figure 5).

We present the satellite time series for two reasons: (i) to affirm an order of magnitude agreement between ground- and space-based observations of Bagana's $SO_2$ emissions, and (ii) to interrogate the long-term trend of emissions since 2017 to the present (i.e. since the analysis of McCormick Kilbride et al., 2019). Rigorous ground-truthing of the satellite data product is not a key goal of our study due to the limited availability of our ground-based data and the challenging measurement conditions we faced (low UV, short observation windows). Moreover, recent efforts to reconcile ground-based remote sensing measurements with emission rates retrieved from TROPOMI data have already demonstrated the potential for good agreement and robust inter-comparison (Theys et al., 2019; Queisser et al., 2019).

We also show infrared data from the Moderate Resolution Imaging Spectroradiometer (MODIS) instrument, processed using the volcanic hotspot detection system MIROVA developed by Coppola et al. (2016, 2020). MODIS provides data in the mid-infrared (MIR: 3.44-4.13 um) about four times per day (two at night and two during the day) at a resolution of 1 km. Incandescent material on the Earth's surface (e.g. lava, whether in flows, domes or lakes) is a strong source of thermal energy in the MIR region of the electromagnetic spectrum, a feature which is used by the MIROVA algorithm to detect the presence of sub-pixel hot sources. The level of MIR radiance above that of the surrounding 'background' landscape is then used to calculate the Volcanic Radiant Power (VRP), a combined measurement of the area of the volcanic emitter and its effective radiating temperature (Coppola et al., 2016). MODIS data is particularly valuable at Bagana as a direct indicator of active lava extrusion (e.g. Wadge et al., 2012, 2018; McCormick Kilbride et al., 2019).

# 3 Results

## 3.1 Volcanic Activity

Bagana was not evidently erupting when we visited in September 2019. Past observations indicate that lava flows are sluggish and that active effusion may be better identified by rockfalls [R.W. Johnson, personal communication]. We observed no incandescence on either summit or flanks and witnessed no ash venting (c.f. McCormick Kilbride et al., 2019). The only evidence of recent eruptive activity was a strongly steaming lava flow on the northern flank, which we observed on arrival in the area by boat and from Piva Government Centre, our first basecamp (Figure 5a, Figure 2). Ephemeral steam emissions are common across the edifice, most likely the result of rainwater evaporating. The persistence of the steaming from the northern flank lava flow may indicate some residual magmatic degassing or simply the current hottest point on the volcano's surface. This flow was probably erupted during an interval of sustained thermal anomalies detected by MIROVA satellite observations in July-December 2018 (Global Volcanism Program, 2019a-c). Specifically, a short period of effusive activity may have occurred around 6 August 2019, when a peak in radiative power over Bagana was detected by the MODIS satellite and a weak thermal anomaly was observed by Sentinel-2 (Massimetti et al., 2020; https://www.mirovaweb.it/?action=volcanoDetails_S2&volcano_id=255020).

Throughout our fieldwork, we observed sustained, dense white emissions from Bagana's summit, with the plume visibly extending several kilometres over the ocean to the west of Bougainville Island (Figure 5a). From images captured by the Titan's on-board action camera, we saw that the plume is composed of emissions escaping from numerous points on the edifice. There is a dense concentration of fumaroles around the summit and more subdued emissions from the fresh lava flow on the northern flank (Figure 5b, Supplementary Figure 1). The majority of the emissions originate from the summit, which is encrusted with white, grey and yellowish mineral deposits (Figure 5c).

Residents of the Wakovi community (Figure 2) reported that no substantial explosive activity has occurred at Bagana since 2014, when hot ashfall ignited house roofs and the community schoolhouse and resulted in temporary self-evacuations to communities near the coast. Villagers reported a number of lines of evidence by which they infer imminent eruptions including vegetation dieback along the upper reaches of the Torokina River due to rising water temperature, presumably a result of heat transfer from rising magmas. The principal risk to the local community results from debris avalanches, including lahars, locally called *tovure*, which pass from the edifice slopes into the upper reaches of the Torokina river. As with our previous visit in 2016 [BTMK], the western approaches to the volcano are covered in thick debris flow deposits, quite distinct from both recent and historic lava flows (Figure 5d).

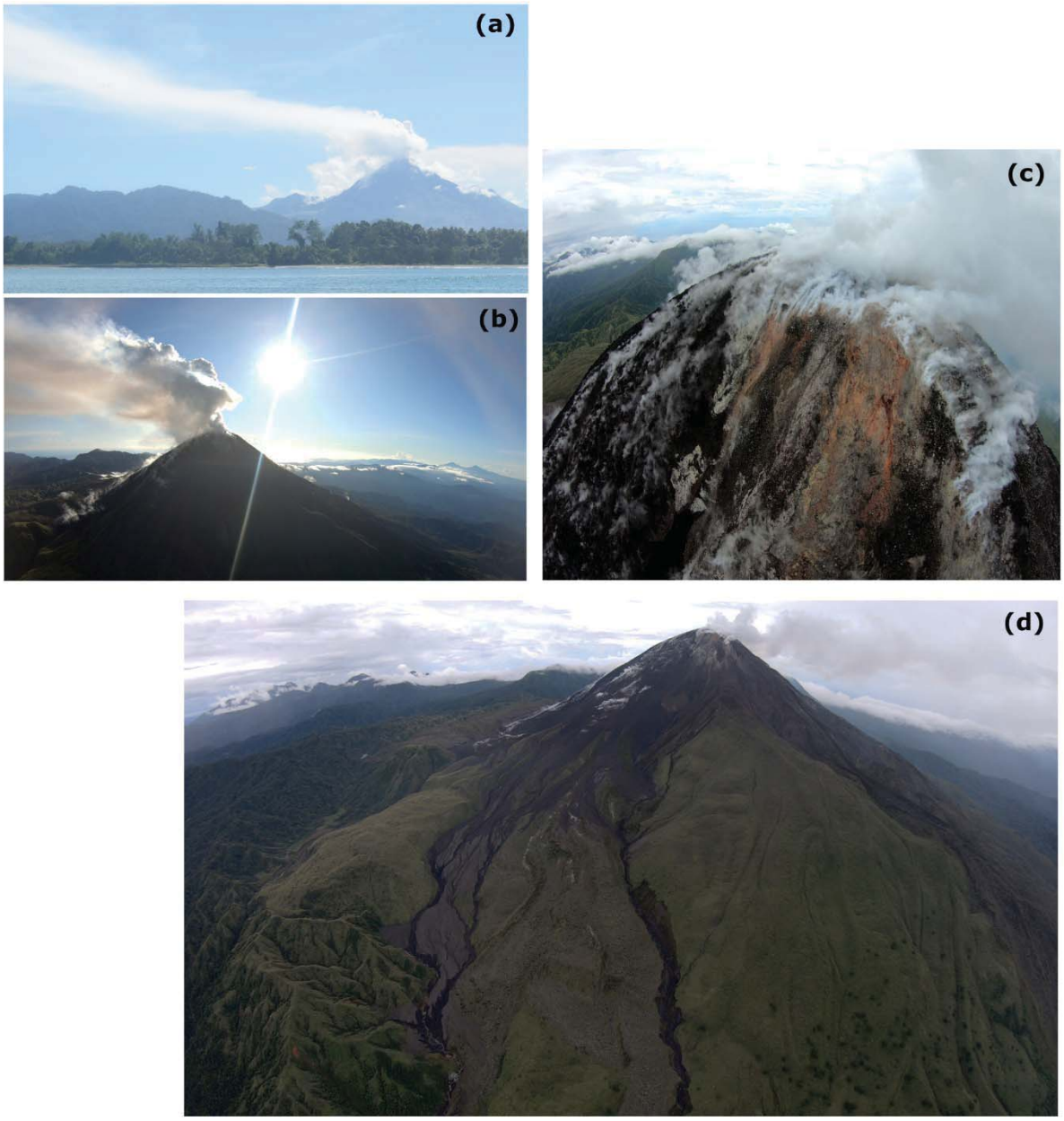


**Figure 5**. (a) View of Bagana and its large gas plume from Paruata Island on 15 September 2019 (Figure 2), around 22 km southwest of the summit. The steaming 2018 lava flow can be seen descending the left flank of the volcano, abutting against the small dome on the skyline. (b) A northeast-ward view from the Titan's forward-facing action camera, taken during the approach to the volcano in Flight 6. Note the strong vertically-rising gas plume and the 2018 lava flow, steaming on the lower left of the image. (c) The summit of the volcano, with extension mineral precipitation and abundant fumaroles. (d) A view from the forward-facing action camera, taken during the approach to the volcano in Flight 4, illustrating the different deposits mantling the edifice. In the lower centre of the image is a large braided lava flow with a rubbly surface that erupted in 2010-12. To the left is a narrow channel of debris avalanche or lahar deposits, which extends several hundred metres further west (behind the aircraft's northeast-ward viewing direction). On the right of the 2010-12 lava flows is a heavily vegetated suite of lava flows erupted from 1957-66 (Wadge et al., 2012). At the extreme right of the image are unvegetated rubbly flows mostly erupted in 2000-05. The lava flows all exhibit prominent channel/levee structures.

### 3.2 Gas Composition

We achieved seven successful flights over Bagana's summit with the Titan UAS (Table 1). Flight 1 was a reconnaissance, with the drone carrying cameras but no gas sensors, in order to trial our flight path, the aircraft endurance, and the local atmospheric conditions. The summit was obscured from our vantage point on the ground by clouds. As the drone passed through these, we made a single pass over the summit, clearing it by around 200 m, and could clearly see (in live-streamed video, Supplementary Figure 1a,b) dense white emissions streaming from multiple points on the summit and appearing to flow down the upper flanks of the edifice.

For Flight 2, we placed the MultiGAS payload aboard the Titan and repeated a similar flight path, cruising around 100 m lower over the summit (1850 m above take-off elevation), and making five passes above the volcano. Our intention was to pass through the plume, having been too high on the previous flight. Visibility on the ground had worsened and from the in-flight video feed (Supplementary Figure 1c,d) we were unable to distinguish meteorological cloud around the summit from any potential volcanic emissions. Despite flying directly over the summit several times, we did not intercept the volcanic plume: the MultiGAS $SO_2$ sensor registered no counts above the noise. During this flight, our Bluedot sensor (P, T, RH) became damaged due to rainwater contact.

We adjusted our flight path for Flight 3, decreasing the Titan's cruising altitude over the volcano to 1800 m above take-off elevation, aiming to ensure the aircraft passed through the gas plume. During the Titan's ascent, thick cloud built up rapidly over the volcano summit and we had zero visibility throughout the flight interval over the summit (Supplementary Figure, 1e,f). We made four passes over the summit, descending by 200 m altitude on the fourth and then passing twice more across the upper flanks. We encountered the plume four times, registering peak $SO_2$ concentrations of 1.1 to 6.2 ppm. However, we have not considered this flight in our analysis because the $CO_2$ data is extremely noisy and never settled on a background value, potentially due to our changing altitude through the gas sensing interval (i.e. non-constant atmospheric pressure during data acquisition). Flight 3 was also the last flight where we made any measurements of pressure, temperature or relative humidity because our backup Bluedot sensor failed, due to prolonged contact with rainwater over the summit.

For Flight 4, we programmed a route comprising three clockwise oblong orbits around the summit, shifting slightly to the south after each, and dropping in altitude from 1800 to 1750 to 1700 m (above take-off) through the course of the flight interval over the summit (Supplementary Figure 4a). The Titan intercepted the gas plume five times during this flight, with clear co-located concentration peaks evident in both our $CO_2$ and $SO_2$ sensor time series (Supplementary Figure 2a). The highest $SO_2$ concentration we measured was 8.1 ppm, during the second of our five plume intercepts; in the remaining four, the peak SO2 concentration ranged from 1.9 to 3.6 ppm. The highest excess $CO_2$ concentration we measured was 98.8 ppm, in the second intercept. Across the full gas sensing interval, we calculate a $CO_2/SO_2$ ratio of $5.6 \pm 2.9$ (Figure 6, Figure 7b). This ratio incorporates a strong positive skew from the second plume intercept, where we calculate $CO_2/SO_2$ of 7.0, in contrast to a range of 1.6 to 2.5 across the four other intercepts (Figure 6). The second intercept occurred when the Titan was directly above the summit (Supplementary Figure 2a), and coincided with the highest $SO_2$ peak measured in Flight 4. As an alternative approach to capturing the overall $CO_2/SO_2$ of Flight 4, a weighted mean

ratio, calculated by weighting each per-intercept ratio by its error (n=5), yields 2.5 ± 8.1. This value lies closer to the ratios calculated from our other flights but is subject to much larger error.

For Flight 5 and Flight 6 we adopted different flight paths to those preceding, namely automated repeated clockwise orbits of the summit (Supplementary Figure 4, Figure 2). Both flights coincided with near-ideal meteorological conditions (Supplementary Figure 1*i-l*). During Flight 5, cruising at 1900 m above take-off elevation, we allowed the Titan to complete six circular orbits (each with a successful plume intercept) before manually piloting the aircraft through three straight traverses over the summit (achieving three further plume intercepts)(Figure 8a-d, Supplementary Figure 4b-j). The geometry of the $SO_2$ concentration peaks measured during plume intercepts varied throughout Flight 5. In the first six plume intercepts, measured during the circular orbits of the summit, the concentration peaks are preceded by a concave downward "shoulder", whereas the final three intercepts, measured during traverses of summit, exhibit peaks with noticeably sharper onsets (Supplementary Figure 2b). This may be a consequence of the circular orbits taking place more or less entirely within the rising gas plume, while the traverses passed from and into plume-free air. We recorded higher peak $SO_2$ and excess $CO_2$ concentrations (up to 12.0 and 72.8 ppm respectively) in the seventh and eight intercepts, perhaps resulting from passing directly through the core of the rising gas plume, as opposed to circling it in the earlier stages of the gas sensing interval (Figure 8a-d, Supplementary Figure 4). Taking the flight as a whole, we calculate a $CO_2/SO_2$ ratio of 3.2 ± 1.0 (Figure 7c). If we differentiate peaks 1-6 and 7-9, based on the different measurement geometry adopted, we calculate $CO_2/SO_2$ of 4.7 ± 1.5 and 2.9 ± 2.0 respectively. The increased error on these ratios does not support a statistically meaningful distinction between the compositions calculated from the two different flight path geometries. The error-weighted mean $CO_2/SO_2$ of the Flight 5 per-intercept ratios (n=9) is 4.1 ± 2.5.

During Flight 6, cruising at 1850 m above take-off elevation, we allowed the Titan to complete seven orbits (with successful plume intercepts) before manually piloting the aircraft through five cross-summit traverses (each with a successful plume intercept)(Figure 8e-h, Supplementary Figure 4k-v). Again, we see a leading shoulder in the $SO_2$ concentration peaks measured during circular orbits (Figure 7). The geometry of the peaks measured during our five plume traverses are more variable. Peaks 8 and 9 are narrow and have sharp onsets. Peaks 10 and 12 (aircraft flying northeastward) however have trailing shoulders, while peak 11 (aircraft flying southwestward) has a leading shoulder. We interpret these as measurements made in the drifting plume rather than the rising plume directly over the summit. We measured our highest peak $SO_2$ and excess $CO_2$ concentrations, ranging from 7.0 to 12.1 ppm and 20.1 to 39.9 ppm respectively, during the traverse interval of flight. Considering the flight as a whole, independently of considerations of either flightpath or gas concentrations, we calculate a $CO_2/SO_2$ of 1.4 ± 0.4 (Figure 7d). If we split the flight into the circular orbits interval (peaks 1-7) and the summit traverse interval (peaks 8-12) we calculate $CO_2/SO_2$ of 1.3 ± 0.6 and 1.5 ± 0.6, which are indistinguishable within error. In contrast with Flights 4 and 5, we do not see a large variation in per-peak $CO_2/SO_2$ ratios throughout Flight 6 (Figure 6a). The error weighted mean $CO_2/SO_2$ across the Flight 6 intercepts (n=12) is 1.3 ± 0.2, which is indistinguishable within error from the ratio obtained by linear fitting the entire Flight 6 dataset.

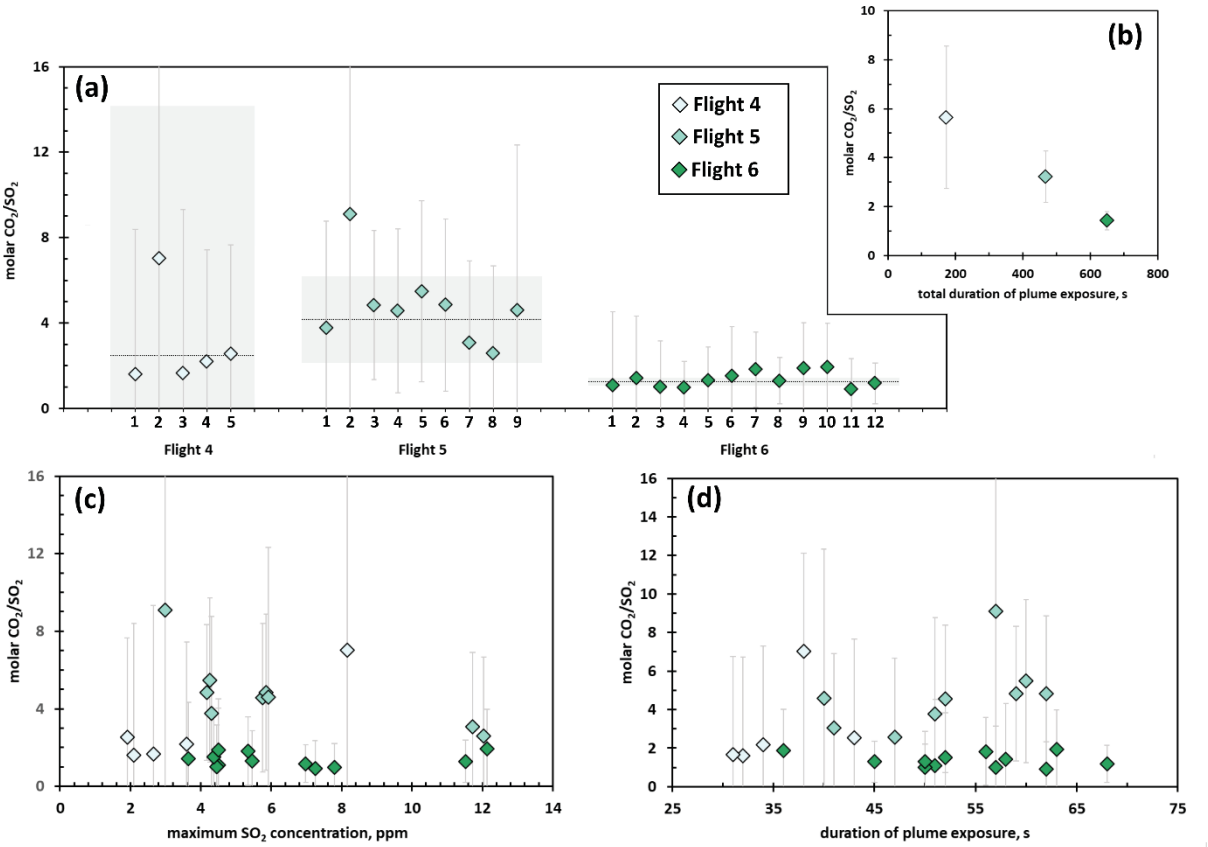


**Figure 6.** (a) The diamond-shaped data points show molar $CO_2/SO_2$ ratios obtained for individual plume intercepts, coloured according to flight. The dashed horizontal lines show the weighted mean $CO_2/SO_2$ ratio obtained by averaging the per-intercept ratios, with the weighting factor based on the per-intercept errors (shown by vertical bars on the diamonds). The shaded panels show the errors on these weighted means.
(b) Molar $CO_2/SO_2$ ratios obtained for each flight, calculated from linear regressions between $SO_2$ and excess $CO_2$ concentration data from all intercepts (Flight 4, n=5; Flight 5, n=9; Flight 6, n=12). Compare with per-flight weighted mean ratios shown by shaded bars in Figure 6a.
(c) Molar $CO_2/SO_2$ ratios obtained for individual plume intercepts, plotted against the corresponding maximum $SO_2$ concentration (ppm) measured during the intercept.
(d) Molar $CO_2/SO_2$ ratios obtained for individual plume intercepts, plotted against the duration of sensor exposure to the volcanic plume.

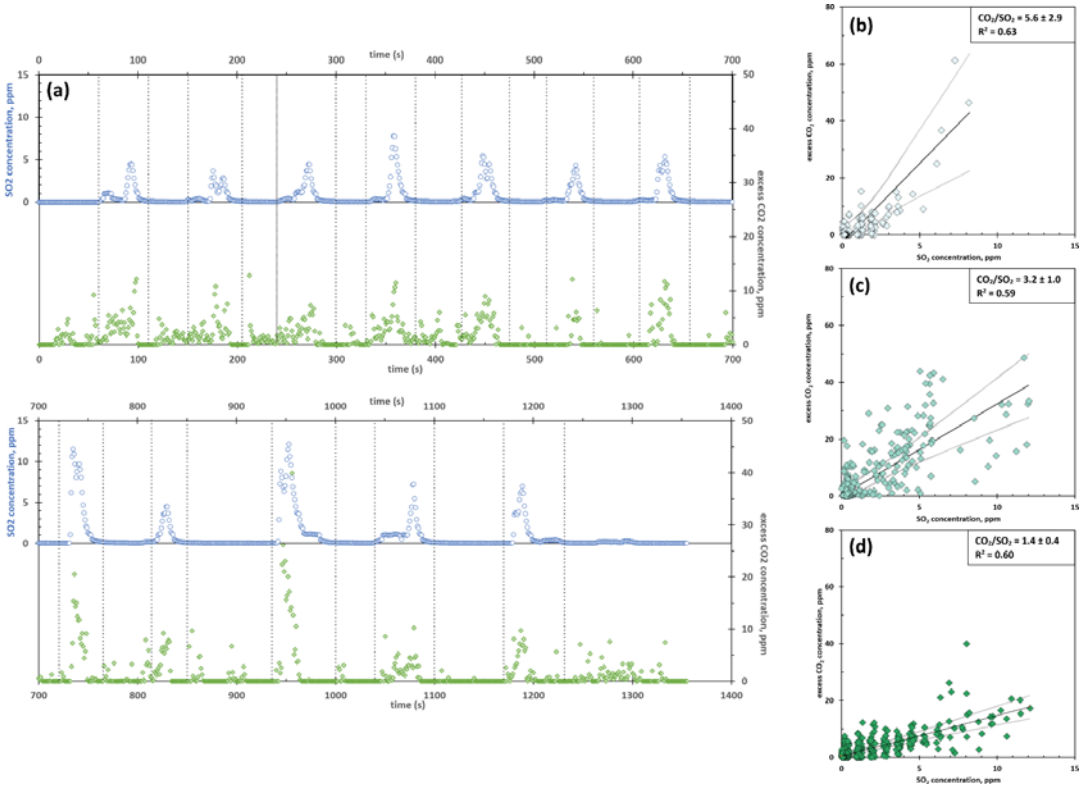


**Figure 7**. (a) Time series of $SO_2$ (blue) and excess $CO_2$ (green) concentrations measured by MultiGAS during intercepts of Bagana's plume during Flight 6, and correlation plots of $SO_2$ and excess $CO_2$ concentrations and molar $CO_2/SO_2$ ratios for (b) Flight 4, (c) Flight 5 and (d) Flight 6. Black lines are the linear regressions from which we derive the ratios; grey lines show the 95% confidence intervals. Vertical grey dashed lines on the time series indicate the 'intercept' intervals ($SO_2$ concentration above the sensor noise) where the UAS flew through the volcanic plume, and which we used to derive per-intercept molar $CO_2/SO_2$ ratios.

| Flight | Date, time (GMT+11) | Max $SO_2$, ppm | Max excess CO2, ppm | $CO_2/SO_2$ | error | n□* | Notes |
|---|---|---|---|---|---|---|---|
| **1** | 16/09/20 17:45 | - | - | - | - | - | Recon. flight without payload |
| **2** | 17/09/20 07:15 | - | - | - | - | - | No plume interceptions |
| **3** | 17/09/20 08:50 | 6.2 | 3.0 | - | - | - | Noisy $CO_2$, did not analyse |
| **4** | 17/09/20 13:15 | 8.1 | 98.8 | 5.6 | 2.9 | 173 | Five plume interceptions |
| | | | | 2.5 | 8.1 | | Weighted mean intercepts 1-5 |
| **5** | 18/09/20 06:45 | 12.0 | 72.8 | 3.2 | 1.0 | 468 | Nine plume interceptions |
| | | *5.9* | 43.8 | *4.7* | *1.5* | *341* | *Intercepts 01-06 only* |
| | | *12.0* | 72.8 | *2.9* | *2.0* | *127* | *Intercepts 07-08 only* |
| | | | | 4.3 | 2.2 | | Weighted mean intercepts 1-9 |
| **6** | 18/09/20 07:40 | 12.1 | 39.9 | 1.4 | 0.4 | 650 | Twelve plume interceptions |
| | | *7.8* | 12.1 | *1.3* | *0.6* | *376* | *Intercepts 01-07 only* |
| | | *12.1* | 39.9 | *1.5* | *0.6* | *274* | *Intercepts 08-12 only* |
| | | | | 1.3 | 0.2 | | Weighted mean intercepts 1-12 |
| **7** | 18/09/20 08:45 | - | - | - | - | - | Abandoned flight due to rain |
| **4-6**[‡] | - | 12.1 | 98.8 | 2.4 | 0.6 | 1311 | Linear regression, 4-6 |
| | | 12.1 | 98.8 | 1.6 | 0.2 | 1311 | Weighted mean, 4-6 |
| | | 12.1 | 98.8 | 1.4 | 0.2 | 674 | Weighted mean, 4-6 ($SO_2$ > 5 ppm) |
| | | 12.1 | 98.8 | 1.6 | 0.8 | 196 | Weighted mean, 4-6 ($SO_2$ > 10 ppm) |

**Table 1.** Summary of our seven gas sensing flights with the Titan UAS. Date and time are in Bougainville local time. *n is the number of measurements (at 1 Hz) used in the calculation of the ratios, effectively equal to the total duration of gas sensor contact with the volcanic plume (in seconds). [‡]This line refers to $CO_2/SO_2$ ratios calculated by incorporating data from Flight 4, Flight 5 and Flight 6.

598 Flight 7 was intended to follow a similar flightpath to Flight 6 but shortly after the UAS reached
599 cruising altitude the weather deteriorated with the onset of heavy rain. Not wishing to risk
600 damage or loss of the Titan or its sensor payload, we abandoned the flight and recovered the
601 aircraft.

602 Figure 6a shows the $CO_2/SO_2$ ratios we calculate for individual plume intercepts. These
603 vary widely and are subject to large uncertainties, due to the low concentrations of gas that the
604 Titan encountered and the short duration of sensor exposure to the volcanic plume. Our
605 deconvolution of the $CO_2$ concentration time series partly compensates for the slow sensor
606 response effects. We do not see strong correlations between per-intercept $CO_2/SO_2$ ratios and
607 peak $SO_2$ concentration (Figure 6c) or exposure time (Figure 6d). In Flight 6, our per-intercept
608 ratios remained relatively stable across a range of $SO_2$ concentration and time spent in the plume,
609 while Flights 4 and 5 show more internal variability. We do see significantly lower errors on the
610 ratios calculated across each flight as the duration of gas-sensor contact increased (Figure 6b).
611 We see no evidence for systematic spatial variations in plume composition (Supplementary
612 Figure 3, 4). Our measured $SO_2$ and excess $CO_2$ concentrations tend to be higher when the UAS
613 was closer to the volcano's summit, but there is no correlation between distance to the summit
614 and instantaneous $CO_2/SO_2$ molar ratio.

615 To derive Bagana's $CO_2$ emission rate (see below), we have to multiply $SO_2$ emission rates
616 measured via UV remote sensing to a representative $CO_2/SO_2$ ratio. The ratio we calculate from
617 our Flight 6 data is subject to lower errors than the Flight 4 and 5 ratios (Table 1) and there is
618 less variation in the per-intercept ratios within Flight 6 (Figure 6a). However, the Titan did
619 unambiguously encounter the volcanic plume several times across Flights 4 and 5. We cannot
620 rule out that the differences in gas composition between each flight are genuinely reflecting
621 spatial or temporal variations in plume chemistry, rather than being consequences of our
622 sampling approach. Therefore, we consider that the overall $CO_2/SO_2$ ratio should be based on as
623 much of our data from these three successful flights as possible. If we combine Flights 4-6 and
624 fit a single linear regression through the data, we obtain $CO_2/SO_2$ of 2.4 ± 0.6. Alternatively, we
625 can calculate a weighted mean $CO_2/SO_2$ ratio of 1.6 ± 0.2 from our (n=26) individual plume
626 intercepts, weighting our calculation according to the error on each intercept, aiming to limit the
627 influence of data with high uncertainty on the overall 'representative' ratio. Note that this is for
628 the purposes of establishing a mean CO2/SO2 only, and not to disregard potential temporal
629 variations in composition between flights. Filtering the data to calculate a ratio from only those
630 plume intercepts where $SO_2$ concentration exceeded 5 ppm (n=12) and 10 ppm (n=4), i.e. those
631 intercepts that are unambiguously 'in-plume' rather than around the diffuse plume margins,
632 yields molar $CO_2/SO_2$ of 1.4 ± 0.2 and 1.6 ± 0.8 respectively, i.e. without significant change in
633 the ratio but with increase in uncertainty.

634

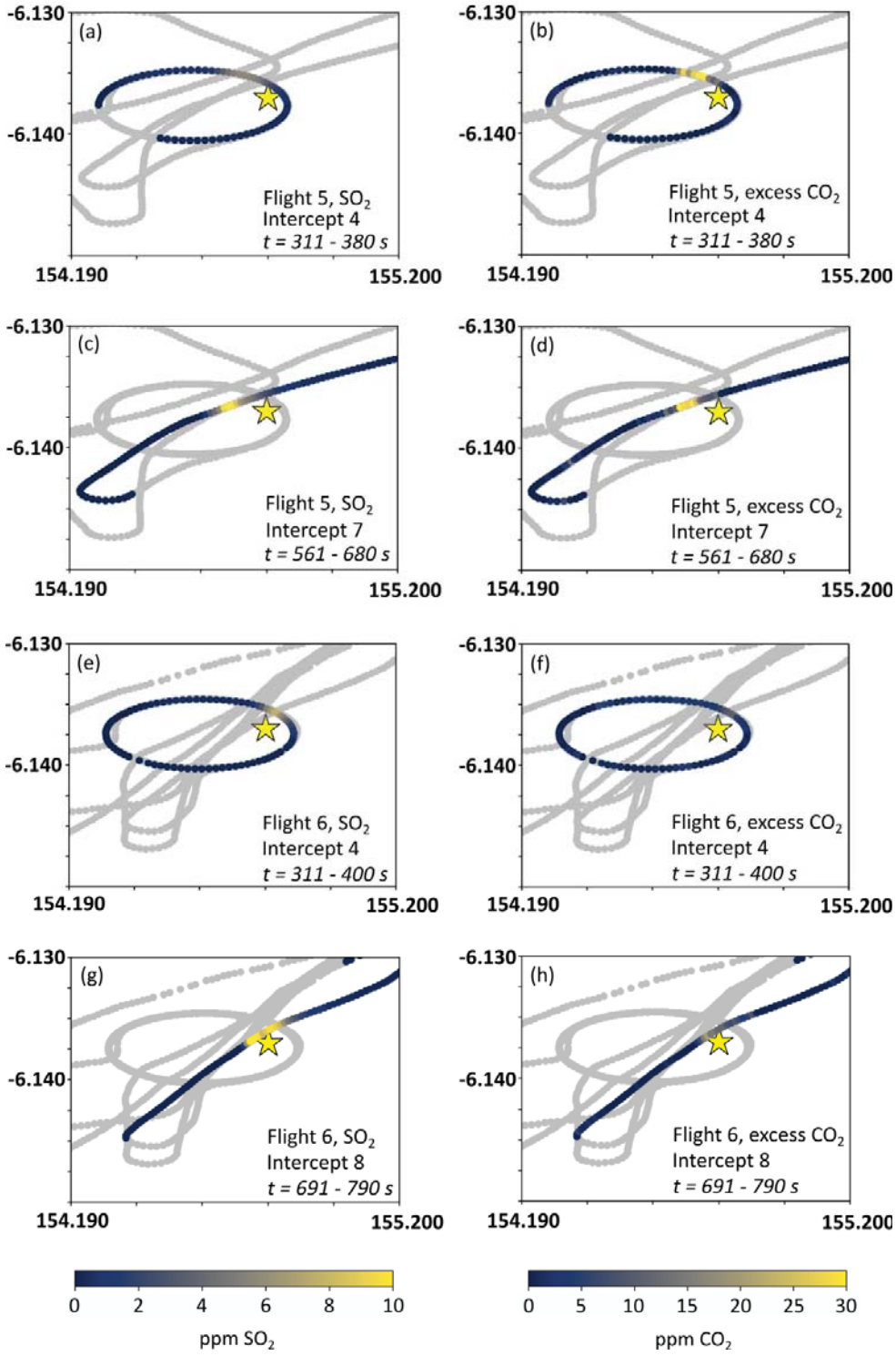


**Figure 8.** Gas concentrations measured by airborne MultiGAS in Flight 5, intercept 4 (a,b) and intercept 7 (c,d) and Flight 6, intercept 4 (e,f) and intercept 8 (g,h). The grey lines show the full path of each flight; colours illustrate the gas concentration, of $SO_2$ (a, c, e, g) and excess $CO_2$ (b, d, f, h). The yellow star represents the volcano's summit. Each map covers the same area; all $SO_2$ panels and $CO_2$ panels respectively have consistent colour scales. The full extent of gas sensing intervals (i.e. plume intercepts) from Flights 4-6 are shown in Supplementary Figure 4.

641 ### 3.3 Sulfur Dioxide Emissions

642 Our most reliable UV camera data comprises around one hour of measurements on the morning
643 of 18 September (first acquisition, 0805-0830; second acquisition 0835-0905) (Figure 9a).
644 Despite relatively low UV levels due to the early time of day, clear skies prevailed over the
645 volcano. Measurement attempts on the previous two days were thwarted by thick cloud cover,
646 rain showers and weak $SO_2$ emissions.

647 We calculate mean (± standard deviation) $SO_2$ emission rates of 4.65 ± 0.28 $kgs^{-1}$ (401 ± 24 $td^{-1}$)
648 in the first acquisition and 3.37 ± 0.37 $kgs^{-1}$ (292 ± 32 $td^{-1}$) in the second (Figure 9a). The
649 apparent decline in $SO_2$ flux through the observation period may be a volcanological
650 phenomenon, though we observed no changes in activity, or a consequence of changing light
651 levels influencing the instrument calibration.

652 We also measured $SO_2$ emissions using mini-DOAS spectrometer traverses (Figure 9b). When
653 close to the volcano on 17 September, our UAS-mounted spectrometer failed to complete a full
654 traverse of the plume. Despite this, we can estimate $SO_2$ emissions from a partial traverse at 380
655 ± 92 $td^{-1}$. If we assume that we captured the majority of the plume, this value should be within
656 error of the true emission rate. As we were leaving the field area by boat on 20 September, we
657 made zenith-pointing traverses with two mini-DOAS instruments. The plume was around 15 km
658 wide at this distance (~35 km) from the volcano summit. The resulting emission rates were 251 ±
659 122 t/d and 234 ± 94 t/d, thus consistent with one another.

660

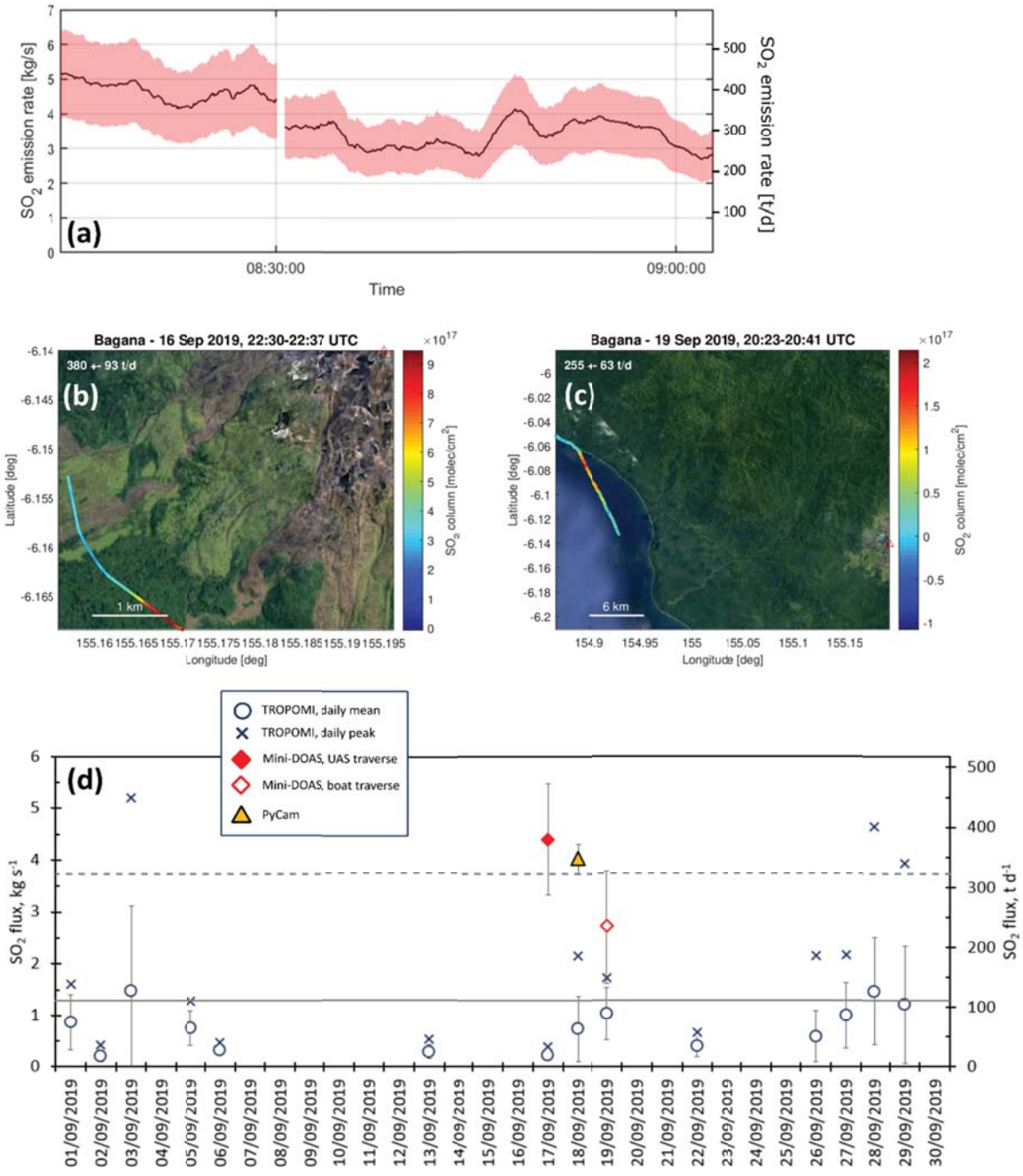


**Figure 9.** (a) Time series of $SO_2$ flux from UV camera acquisition on morning of 18th September 2019, with one sigma uncertainty about the calculated flux value; (b) Maps of $SO_2$ vertical column density measured by mini-DOAS in traverses by multi-rotor UAS (left, 17th September 2019) and boat (right, 20th September 2019). (c) Composite daily $SO_2$ emission rate time series through September 2019, incorporating TROPOMI satellite observations and the ground-based remote sensing data we collected during our fieldwork. Horizontal dashed line shows the mean $SO_2$ emission rate from ground-based data; horizontal solid line shows the mean $SO_2$ emission rate from satellite-based data.

672 ### 3.4 Satellite Observations of Gas and Thermal Emissions

673 TROPOMI observations allow us to quantify $SO_2$ emissions from May 2018 to February 2022
674 (Figure 10, Figure 11, Supplementary Figure 5a-l). Over this interval, we obtained an estimate of
675 mean daily $SO_2$ flux on 885 days, of which 453 days saw the mean flux exceed 1.0 kg $s^{-1}$.
676 TROPOMI failed to detect a plume from Bagana on 505 days, due either to emissions dropping
677 below the sensor's resolution, cloud cover, or none of our PlumeTraj trajectories returning to
678 Bagana. In September 2019, we have fourteen days with estimates of $SO_2$ flux, with an average
679 of 0.75 kg $s^{-1}$ (65 $td^{-1}$) and a maximum peak daily flux of 5.20 kg $s^{-1}$ (450 $td^{-1}$). Generally, our
680 satellite-based emission rates in September 2019 are lower than those we measured by ground-
681 based remote sensing in the field (Figure 9d). We are unable to evaluate rigorously whether this
682 is due to different sensitivities, measurement geometries, or time or duration of measurement
683 (i.e. satellite-based fluxes are constructed over several hours, our ground-based measurements
684 each cover < 1 hour). The mean (± S.D.) $SO_2$ emission rate in September 2019 if we combine
685 our satellite and ground-based measurements is 116 ± 118 $td^{-1}$. This is lower than the mean of the
686 ground-based measurements we made during our fieldwork and may be due to lower activity and
687 emissions in the remainder of the month, or a low bias resulting from reduced TROPOMI
688 sensitivity during periods of lower emissions (e.g. low altitudes, low vertical column densities).

689 Our satellite observations suggest three broad phases of contrasting activity at Bagana since
690 2018: (i) from May to December 2018, $SO_2$ emissions are relatively high with mean (± S.D.)
691 daily emissions per month ranging from 100 ± 70 to 520 ± 348 $td^{-1}$; (ii) from January 2019 to
692 March 2021, $SO_2$ emissions are relatively low with mean daily emissions below 100 $td^{-1}$ in every
693 month except August and December 2019; and (iii) since March 2021, $SO_2$ emissions are
694 relatively high again, with mean daily emissions per month ranging from 123 ± 109 to 498 ± 350
695 $td^{-1}$ (Figure 10a). The large relative magnitude of the standard deviation to the mean points to
696 high inter-daily variation in $SO_2$ emission rates (Figure 10b). Independent observations from the
697 MODIS thermal infrared sensor, processed with the MIROVA algorithm (Coppola et al., 2016,
698 2020) support the notion of three periods of activity, with elevated thermal emissions in May-
699 December 2018 and since March 2021, with an intervening period largely characterised by the
700 absence of thermal emissions (Figure 10c). Peak $SO_2$ plume heights, another output of our
701 PlumeTraj routine, do not show systematic variations with either $SO_2$ emission rate or thermal
702 flux, but tend to lie between 2-5 km for the entire study interval (Figure 10d).

703

704

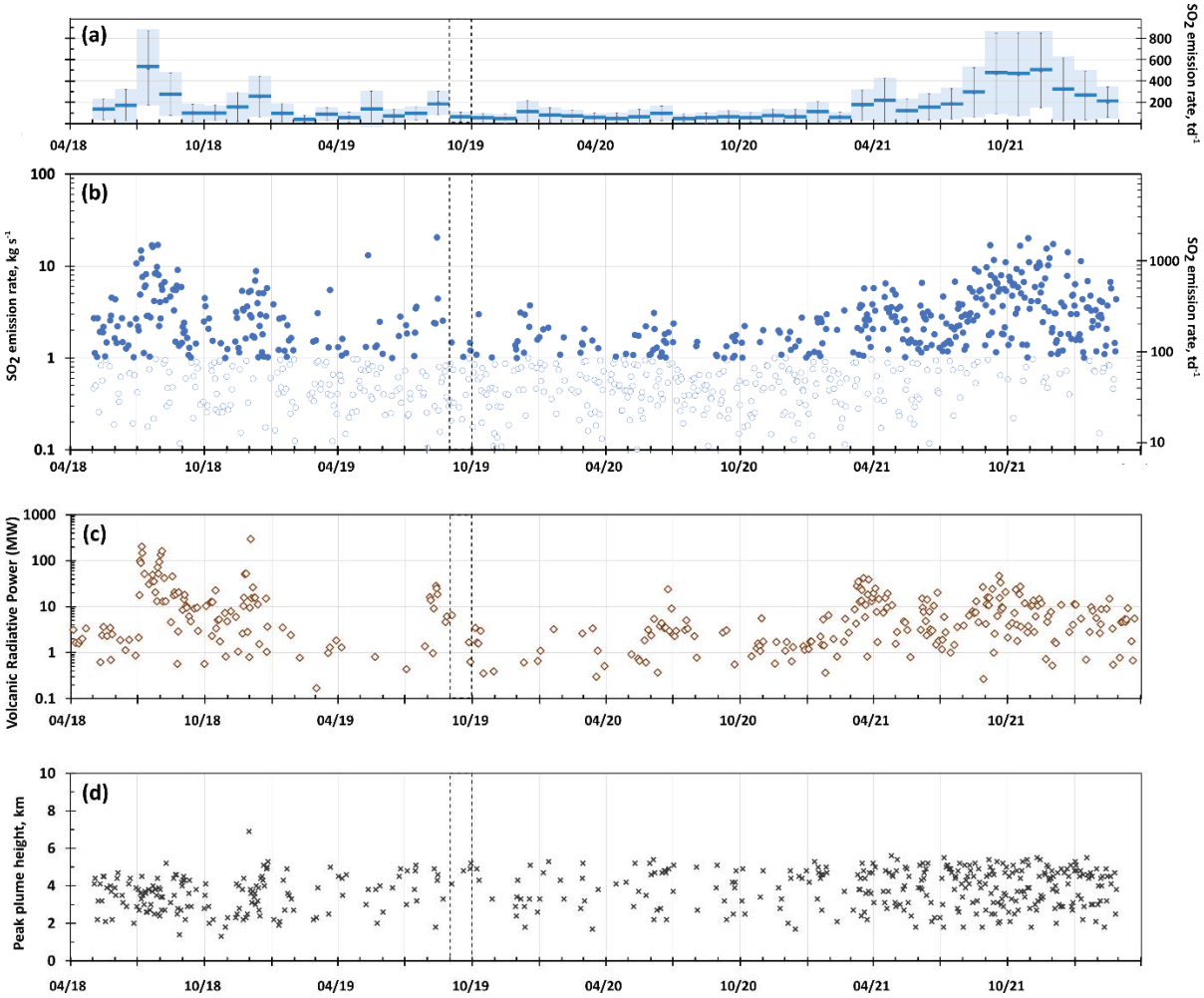


**Figure 10.** Satellite observations of Bagana's activity from May 2018 to present. (a) Mean (± standard deviation) $SO_2$ emission rate for each month of our study interval, derived from TROPOMI observations; (b) daily mean $SO_2$ emission rates retrieved from TROPOMI observations, with days where flux is below 1.0 kg $s^{-1}$ (~90 $td^{-1}$) and thus subject to greater uncertainty shown in paler colours; (c) volcanic radiative power, expressed in MW, obtained from the MIROVA system's analysis of MODIS thermal infrared retrievals over Bagana; (d) Maximum plume height retrieved per day, obtained from PlumeTraj analysis of TROPOMI retrievals. In each panel, the vertical black dashed lines highlight September 2019, when our fieldwork took place.

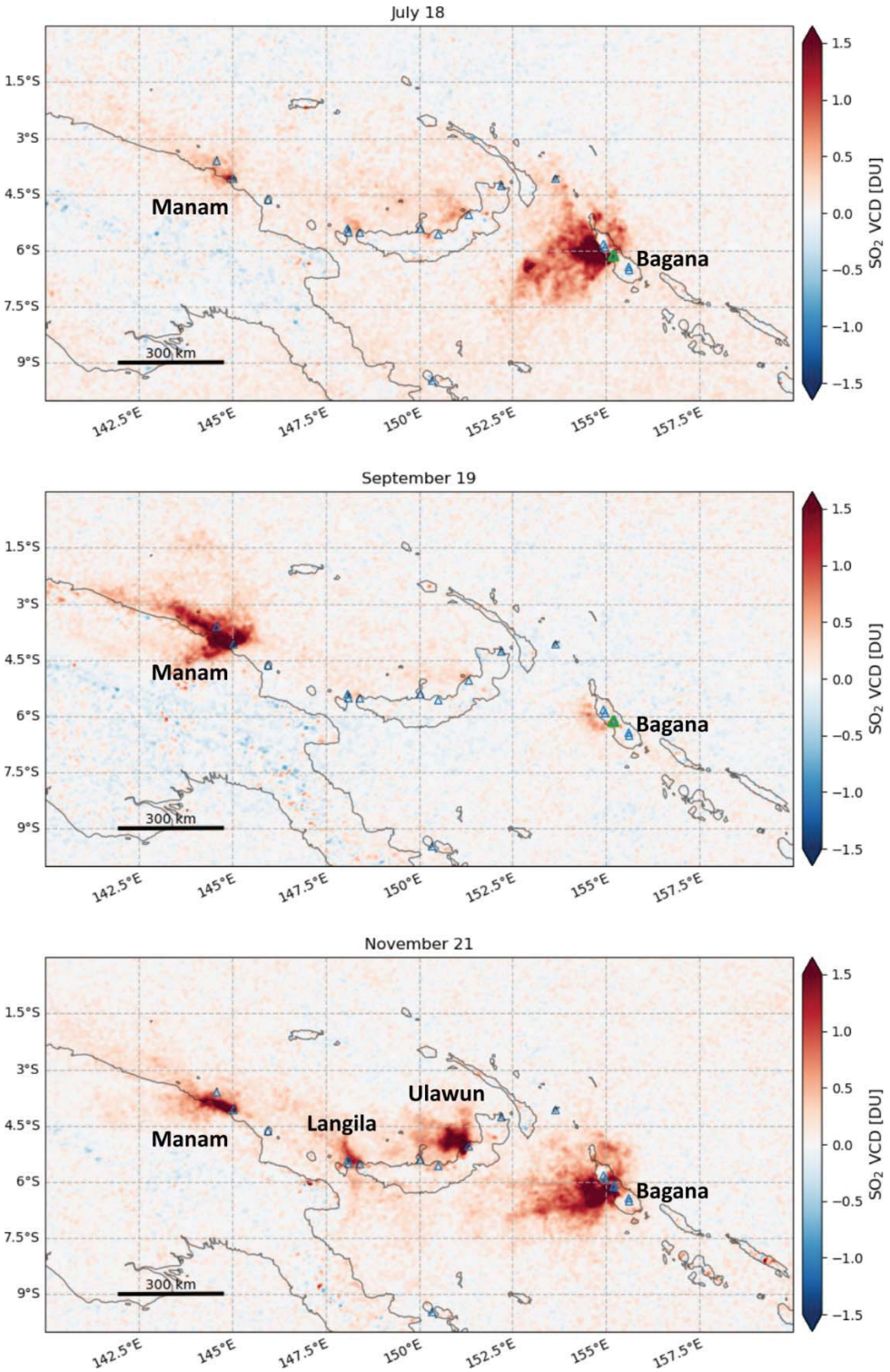


**Figure 11.** Average atmospheric $SO_2$ vertical column densities over Papua New Guinea, as observed by TROPOMI for July 2018 (top), September 2019 (middle) and November 2021 (bottom). We construct these maps by averaging all TROPOMI observations acquired in each month. In July 2018 and November 2021, Bagana was in a state of active lava extrusion accompanied by elevated $SO_2$ gas emissions. In September 2019, coincident with our field campaign, Bagana was in much lower state of activity (no visible eruption) and reduced gas emissions. Note $SO_2$ emissions of varying strength from other volcanoes across the region: Manam, Langila and Ulawun.

# 4 Discussion

## 4.1 Carbon and Sulfur Fluxes from Bagana, and Implications for Regional Emissions Budgets

The molar $CO_2/SO_2$ ratio for Bagana's plume is 2.4 ± 0.6 if we calculate it via a single linear regression through all our MultiGAS data from Flights 4-6, or 1.6 ± 0.2 if we calculate it via an error-weighted mean of our 26 per-intercept $CO_2/SO_2$ ratios. The 'combined linear regression ratio' may obscure temporal variation in gas composition between each flight, while the 'error-weighted mean ratio' more explicitly accounts for temporal variations. Our error weighting of the mean compensates for the short duration of individual plume intercepts.

Our data ($CO_2/SO_2$ = 1.6 ± 0.2) suggest Bagana's gas emissions are carbon-poorer than, but overlap within error with, the composition ($CO_2/SO_2$ = 2.4 ± 0.7) predicted from global relationships between $CO_2/SO_2$ in high temperature volcanic gas emissions and Ba/La (or Sr/Nd) in erupted rocks (Aiuppa et al., 2019). All Papua New Guinea's volcanoes, including Bagana, were assigned to 'Group 2', volcanoes characterised by relatively carbon-rich emissions due to efficient recycling of slab carbon into the sub-arc mantle. Whether this is true for Bagana remains open to debate. There are no direct samples of the subducting slab in the Solomon Sea (e.g. piston cores seaward of the Bougainville trench), just dredges and a free-fall grab from the *R.V. Natsushima*'s 1983-84 cruise (Crook, 1987; Woodhead et al., 1998). The sampled lithologies comprise volcaniclastic sediments, mudrocks and only minor limestones. It is not clear how well these samples reflect the slab composition at sub-arc depths. Trace element (e.g. Th/Yb vs Sr/Nd) and radiogenic isotope (i.e. Sr-Nd-Pb) data for lavas from Bagana and other Bougainville volcanoes suggest a fluid-dominated slab flux and only minor sedimentary influence (Hergt et al., 2018; J. Woodhead, pers. comm., McCormick Kilbride, unpublished data). This may explain our relatively carbon-poor gas compositions, but further work is required to characterise volatile provenance in this arc segment.

The gas composition predicted by Aiuppa et al. (2019) is based on the chemistry of lavas erupted over decades (Bultitude, 1982). Our data are direct measurements of Bagana's emissions but represent just two days of relatively low-level activity for this volcano. This considered, the fact the two estimates match within error is perhaps surprising. Volcanoes can exhibit dramatic temporal changes in gas composition, with $CO_2/SO_2$ increasing following mafic recharge into shallow crustal reservoirs or as unrest builds prior to eruptions (e.g. Aiuppa et al., 2007; Werner et al., 2019). Our data do not allow us to predict whether Bagana's gas composition might vary as a function of activity, but it seems plausible that co-eruptive emissions may differ in composition to the gases we measured in September 2019, a period of relative quiescence. If we consider a general degassing model of andesitic volcanoes (e.g., Edmonds et al., 2022) that sees surface gas emissions as mixtures of deeply-exsolved ($CO_2$-rich) fluids delivered largely through second boiling of intruded hydrous magmas, and more S-rich fluids released during shallow crystallization or ascent and extrusion, we may interpret our relatively low measured $CO_2/SO_2$ as the product of residual degassing of shallow-stored magma that ascended to the upper reaches of Bagana's plumbing system but was not erupted. Thus, while our calculation of $CO_2$ emission rates relies on our measured $CO_2/SO_2$ ratio, we note that this may not closely resemble Bagana's 'true' long-term gas composition.

766 We measured Bagana's $SO_2$ emission rate using a combination of a UAS traverse with mini-
767 DOAS, a boat traverse with mini-DOAS, the PiCam, and TROPOMI satellite observations
768 (Figure 9c). The mean (± standard deviation) $SO_2$ emission rate from our ground-based
769 measurements (PiCam and mini-DOAS) is 320 ± 76 $td^{-1}$. These are the lowest emissions rates yet
770 measured at Bagana. Earlier campaign measurements reported $SO_2$ fluxes of 3100 $td^{-1}$ in 1983
771 and 3200 $td^{-1}$ in 1989, 1900 $td^{-1}$ in 2003, and 3900 $td^{-1}$ in 2016 (Global Volcanism Program,
772 1983, 1989; McGonigle et al., 2004; D'Aleo et al., 2017). Multi-year satellite observations have
773 also suggested typical $SO_2$ emissions of $\geq 10^3$ $td^{-1}$ from 2005-18 (Carn et al., 2017; McCormick
774 Kilbride et al., 2019).

775 Since 2018, our new satellite observations suggest three intervals of differing behaviour, defined
776 above in terms of $SO_2$ and thermal emissions as: (i) May to December 2018; (ii) January 2019 to
777 March 2021; (iii) March 2021 to present. Our interpretation of these three intervals is that the
778 first and third represent episodes of lava extrusion, while the second is a period of quiescence
779 accompanied by passive $SO_2$ emissions (Figure 10). Elevated gas emissions accompanying
780 active extrusion, interpreted from a striking correspondence between $SO_2$ and thermal emissions
781 seems to be a characteristic feature of Bagana (Wadge et al., 2018; McCormick Kilbride et al.,
782 2019) and is further evident in activity reports compiled by the Smithsonian Global Volcanism
783 Program. The first interval of elevated gas and thermal emissions is likely to have coincided with
784 the extrusion of the fresh lava flow we observed in Bagana's northern flank during our fieldwork
785 in September 2019. In spring 2021, thermal anomalies were detected by the Sentinel-2 satellite,
786 initially confined to the summit area before spreading to the northern flank (Global Volcanism
787 Program, 2021a,b). At the time of writing, we assume this lava extrusion may still be ongoing
788 (https://www.mirovaweb.it/?action=volcanoDetails_S2&volcano_id=255020). Overall, our $SO_2$
789 data from September 2019 are consistent with the general decline in activity at Bagana since
790 2012 (McCormick Kilbride et al., 2019; Global Volcanism Program, 2019a, 2019b, 2019c,
791 2020). The volcano exhibits a wide range in the intensity of its activity (further borne out by our
792 satellite data in this study, Figure 10, Figure 11, Supplementary Figure 5a-l) and our field
793 campaign coincided with a period of particularly low-level unrest.

794 $SO_2$ emissions at relatively quiescent volcanoes can also decrease due to scrubbing, that is, the
795 interaction of rising gas with groundwater in fractures in the volcanic edifice. The Bagana edifice
796 is likely to be partly saturated with water, owing to heavy daily rainfall. There are numerous
797 fumaroles on the summit rather than a single 'open vent', extensive mineral precipitation around
798 these fumaroles, and faint odours of sulfur in the small rivers around the volcano (Figure 5c).
799 However, we did not detect any $H_2S$ in the Bagana gas plume, which we would expect under
800 conditions of significant scrubbing, due to $SO_2$ hydrolysis (Symonds et al., 2001). Thus, we
801 judge our $SO_2$ emission rates to be reflective of Bagana's reduced activity at the time of
802 sampling, rather than the effect of scrubbing.

803 A molar $CO_2/SO_2$ ratio of 1.6 ± 0.2 is equivalent to a mass ratio of 1.1 ± 0.1. Multiplying this by
804 our mean ground-based $SO_2$ emission rate of 320 ± 76 $td^{-1}$ yields a $CO_2$ flux of 320 ± 84 $td^{-1}$.
805 This is our best estimate for Bagana's carbon emissions at the time of measurement in 2019,
806 given the comparable temporal duration of our UAS-based plume composition data and our
807 ground-based $SO_2$ emission rate data. Considering September 2019 as a whole, and our
808 combined satellite plus ground-based $SO_2$ emission rate data, we estimate a $CO_2$ emission rate of
809 128 ± 130 $td^{-1}$. This estimate is subject to two key uncertainties, namely the assumption of fixed

$CO_2/SO_2$ throughout the month, and whether the ground- and satellite-based estimates of $SO_2$ emissions can be seamlessly combined. The potential influence of these uncertainties only grows if we extrapolate our data over longer timescales.

We can calculate a long-term (i.e. multi-year) estimate of $CO_2$ emissions from Bagana by combining our campaign $CO_2/SO_2$ (mass ratio of 1.1 ± 0.1) with our mean (± standard deviation) $SO_2$ flux from TROPOMI observations in 2018-2022 (175 ± 234 $td^{-1}$). The resulting value of $CO_2$ flux, 193 ± 257 $td^{-1}$, and our campaign-only value of 320 ± 84 $td^{-1}$, are significantly lower than the value of 6245 ± 2335 $td^{-1}$ predicted by Aiuppa et al. (2019), who placed Bagana as Earth's fifth ranked volcanic carbon source. The $CO_2/SO_2$ ratio (2.4 ± 0.7, predicted as described above) and the $SO_2$ flux (1032-1971 kt $yr^{-1}$, from satellite observations in 2005-15 presented by Carn et al., 2017) used by Aiuppa et al. (2019) in their computation of $CO_2$ flux are significantly higher than the values we measured in September 2019. Thus, our derived $CO_2$ emission rate is substantially lower and, in September 2019 at least, Bagana is unlikely to have been a significant contributor to global volcanic carbon emissions. During intervals of elevated activity, however, Bagana may indeed be one of Earth's most important volcanic carbon emitters. Fresh magmas fed into the shallow reservoirs from depth are likely to release relatively carbon-rich gas (with $CO_2/SO_2$ perhaps comparable to Aiuppa et al. (2019)'s predicted value of 2.4 ± 0.7). We know co-eruptive $SO_2$ fluxes at Bagana can exceed $10^4$ $td^{-1}$ (this study, McCormick Kilbride et al., 2019, and references therein). Thus, peak $CO_2$ emissions at Bagana may be up to two orders of magnitude greater than what we measured in September 2019.

The foregoing discussion exemplifies a major challenge: how to accurately quantify global volcanic emissions when individual volcanoes have emissions that vary widely through time. Recent attempts to quantify global volcanic sulfur (Carn et al., 2017) and carbon emissions (Aiuppa et al., 2019; Werner et al., 2019; Fischer et al., 2019) partly agree with earlier studies (e.g. Andres & Kasgnoc, 1998) that certain volcanoes tend to rank highly from year to year, and from decade to decade. However, many other volcanoes once considered globally important sources of volatiles into the atmosphere are now exhibiting reduced activity and more modest emissions. Miyakejima, in the northern Izu-Bonin arc, was among the world's major $SO_2$ emitters following its effusive eruption in 2000 before an exponential drop in outgassing through the following decade (Kazahaya et al., 2004; Mori et al., 2013; Carn et al., 2017). Anatahan, in the Mariana arc, likewise retains a high ranking in global emissions inventories (Carn et al., 2017; Aiuppa et al., 2019), notwithstanding the fact that ~85% of its $SO_2$ flux over the past three decades coincided with short-lived, intense eruptions, mostly in January-August 2005 (McCormick et al., 2015). Kilauea volcano on Hawaii has been a prodigious source of gas into the atmosphere for decades, yet following the end of the 2018 East Rift Zone eruption, $SO_2$ emissions fell below 100 $td^{-1}$ (Elias et al., 2018; Kern et al., 2020). Conversely, Turrialba volcano in Costa Rica, awakened from a lengthy repose in 2018 and now dominates $SO_2$ and $CO_2$ emissions in the Central American Volcanic Arc (de Moor et al., 2017, c.f. Mather et al., 2006, and references therein). These data, and the picture of Bagana we present herein, illustrate that highly variable gas emission rates (and potentially composition, too) is inherent to many volcanoes and this fact could, and should, be better incorporated into volcanic emissions inventories.

Quantifying the temporal variability of volcanic emissions over longer timeframes is essential if we are to fully evaluate the influence of volcanic outgassing to the composition of Earth's

atmosphere and consequently to planetary climate. The period of observations at volcanoes is still relatively short compared to the cycles of activity (Werner et al., 2019). Short duration campaign datasets will seldom fully characterise highly dynamic systems and it follows that many volcanoes worldwide are inadequately characterised in terms of their outgassing flux and that many of our measurements are biased because they are often made during the most active periods (Werner et al., 2019). Long-term, more sustained and integrated emissions monitoring is required, melding synoptic satellite observations, automated ground-based remote sensing, permanently installed MultiGAS stations, regular sampling and analysis of emitted gases, and a key role for UAS in acquiring measurements and samples from otherwise inaccessible gas plumes (James et al., 2020; Edmonds, 2021; Kern et al., 2022).

### 4.2 Aerial Strategies for Volcano Monitoring

Our adoption of UAS to carry a gas sensor payload into Bagana's otherwise inaccessible summit plume has enabled the first measurement of gas composition and $CO_2$ outgassing from this volcano. Alongside other recent studies, this is a clear demonstration of the great potential offered by UAS in volcanic gas monitoring and research (Stix et al., 2018; James et al., 2020; Liu et al., 2020a; Pering et al., 2020; Shinohara et al., 2020). In particular, drones operating beyond visual line of sight (BVLOS) enable safe access to plumes from a distance of several kilometres, ensuring safety for operators and reducing the need to climb potentially unstable edifices to access summit vents directly (Schellenberg et al., 2019; Liu et al., 2020a; Wood et al., 2020).

Our aircraft made several successful traverses of the Bagana plume and we consider our work herein as further valuable evidence that UAS operations with a dedicated MultiGAS payload can recover volcanic plume gas composition robustly. Challenges do remain. Our MultiGAS data sets are of shorter duration than is typical for ground-based studies, where the instrument is placed within the plume directly and may be left for several days or installed permanently (e.g. Aiuppa et al., 2007, de Moor et al., 2016). Flying in a dilute plume meant that our instruments encountered relatively low gas concentrations over Bagana (c.f. our experience of a more 'open vent' system at Manam, Liu et al., 2020a) but this is an inherent feature of airborne sampling versus ground-based MultiGAS deployments (Werner et al., 2013; Fischer & Lopez, 2016). Multi-rotor aircraft, rather than the fixed-wing Titan, offer more potential for sustained plume exposure, owing to their ability to hover in place. However, multi-kilometre horizontal flight or vertical ascent and descent with a multi-rotor are costly in terms of battery power, and the addition of more batteries to the aircraft payload greatly increases the takeoff weight. The Titan cruises at roughly 20 $ms^{-1}$ which allowed us to reach the volcanic summit plume relatively quickly and, by largely gliding on the inbound leg of its flight, enabled us to expend more battery power over the summit, thus increasing plume exposure times. Thermal energy in buoyant volcanic plumes may help to extend endurance further by reducing power consumption during summit traverses (Wood et al., 2020). In future, vertical take-off and landing (VTOL) aircraft may offer a combination of the fixed-wing flight into a volcanic plume from a distance of several kilometres, accompanied by a relatively prolonged gas-sensing interval hovering in the plume. For now, potential uncertainties in gas composition arising from short sensor exposure to the volcanic gas can be overcome, as here, by repeated flights and by manual traverses within each

flight to maximise gas contact. Through our three successful flights, increasing time spent in the plume did demonstrably lead to decreased uncertainty on our recovered $CO_2/SO_2$ ratio (Figure 6b,d), although we cannot rule out that differences in the absolute value of the ratio from each flight are the result of spatial or temporal variations in gas composition.

Successful recovery of any UAS after exposure to a distant and potentially turbulent airspace is no small feat, with changing volcanic activity potentially resulting in aircraft loss (Wood et al., 2020). Each successful flight within a campaign therefore provides opportunities to improve flight operations iteratively and reflect on aircraft design to ensure safe aircraft recovery. Our work on Bagana directly followed our previous work on Manam and allowed us to explore our UAS capability further. One challenge we experienced was a telemetry shadow when the volcanic edifice lay between our ground station and the aircraft. We modified the geometry of our flight plans to minimise the time that the Titan spent in this radio 'dead zone'. We also flew much closer to the volcanic summit than we had on Manam, at one point passing within 50 m altitude of the summit in pursuit of elevated gas concentrations. To achieve such close passes without aircraft loss requires high resolution and up-to-date topographic models for flight planning, which can be challenging to obtain for volcanoes with summit lava domes where active extrusion can modify topography by tens of metres. Moreover, a skilled pilot must monitor the in-flight FPV feed and be ready to take manual control in the event of obstacles, turbulence or other threats to the aircraft. A full review of design requirements for successful fixed-wing UAS deployments is provided by Wood et al. (2020), resulting from volcanological fieldwork in recent years (Schellenberg et al., 2019; Liu et al., 2020a; this study).

### 4.3 Future Volcano Monitoring at Bagana

Bagana is a remote volcano with no instrumented ground-based monitoring. A local observer is retained by Rabaul Volcanological Observatory to provide semi-regular radio reports of changing activity and various community leaders liaise with the Bougainville Disaster Office in terms of both observations of activity and discussions for hazard mitigation and disaster risk reduction. The typical eruptive activity at Bagana, sluggish lava flows that are generally restricted to the cone, pose little direct hazard to populations in the surrounding villages (Figure 2). Of more concern are rare explosive eruptions which deposit hot ash on buildings, leading to fires and, more commonly, debris avalanches from the edifice into the upper reaches of the Torokina river. These flows are dynamic and powerful, based on local testimony and the large boulders and trees we observed in the riverbeds.

In the absence of monitoring instruments, the main mitigation measures at Bagana are visits by RVO and BDO personnel to raise awareness among local communities of volcanic hazards. From our experience in the Wakovi and Piva communities, the level of hazard awareness is high among local people, with significant inter-generational memory of a range of activity styles. Moreover, a number of people described to us precursory phenomena they associate with imminent eruptions. This knowledge is among several factors influencing these communities' resilience: strong kinship relations with adjacent communities ensure alternative dwelling places may be sought in times of elevated activity, and families can mobilise and evacuate quickly. The major caveat to this perspective is how the level of risk (and capacity for mitigation) might vary

in more unusual activity, for example, the rare, high intensity explosive eruptions accompanied by pyroclastic flows known from Bagana's eruptive history (Bultitude et al., 1978). It remains unknown why these events occur. Possibilities include mafic recharge introducing volatile-rich magma into the shallow plumbing system (e.g. Roberge et al., 2009), changes in supply of gas from deeper reservoirs into the shallow plumbing system (e.g., Liu et al., 2020b; Edmonds et al., 2022), or hydrothermal mineralisation sealing fractures in the summit dome and generating overpressure in the slowly degassing magma beneath (e.g., Heap et al., 2021). The scarcity of these events and therefore the limited experience of local communities in witnessing characteristic precursory behaviour increases community vulnerability. In our discussions with Wakovi residents, a recurring suggestion we heard was that the absence of a strong visible gas plume from Bagana's summit would be perceived unusual or uncharacteristic and potentially taken as evidence of an imminent eruption; this was usually illustrated via the analogy of a steaming cooking pot with a closely fitting lid.

The BVLOS measurements we describe herein require a skilled pilot and access to electronic components, so are not, in our judgment, yet feasible for regular monitoring in isolated locations such as the interior of Bougainville. Less complex UAS operations, such as deploying commercially available multi-rotor aircraft for observations of changing unrest or edifice stability (e.g. accumulation of avalanche material on upper slopes) might be more feasible at Bagana. Regular UAS-based surveillance and measurements of volcanic emissions have been recently adopted by RVO at other volcanoes, notably gas sensing flights at Rabaul and observations of the evolving lava flow hazard during the 2019 Ulawun flank fissure eruption. For now, a more realistic monitoring strategy for remote volcanoes in PNG may be the provision of satellite data to RVO, in near-real-time, that could be relayed to BDO or even communities in the Torokina region for dissemination to the surrounding villages. Such a strategy faces its own challenges, in terms of resourcing the regular analysis of satellite observations, timely and accurate transmission to RVO, data storage and processing capacity at the observatory, and reliable radio transmission to the remote interior of Bougainville. These challenges are set within a complex geopolitical context, with regional and national governments presently engaged in negotiations over the potential secession of Bougainville from Papua New Guinea. The foregoing discussion serves to illustrate the numerous challenges facing monitoring of remote volcanoes, particularly those capable of sustained eruptive activity, and also to emphasise the important and sometimes underappreciated role of local resilience measures in safeguarding populations from volcanic hazards..

## 5 Conclusions

We used UAS to fly a custom-built MultiGAS instrument into the summit plume of Bagana, a remote and persistently active volcano, and achieved the first measurements of the composition of Bagana gas emissions. We have demonstrated, building on our previous work, that fixed-wing UAS operating beyond visual line of sight are a powerful tool to study emissions from otherwise inaccessible vents. The short residence times we achieved in the plume (e.g. relative to conventional ground-based MultiGAS deployments) can be compensated for by repeated flights intercepting the plume. The uncertainties on our obtained plume composition data diminish with increased plume exposure, but such integration limits our ability to reconstruct temporal or spatial variations in gas composition. In future work, we aim to overcome these challenges, for example by developing aircraft that can hover or otherwise maintain prolonged contact between the gas sensor payload and the volcanic plume.

By combining our plume composition data with coincident remote sensing measurements of $SO_2$ emissions, we have derived a first estimate of $CO_2$ flux from Bagana, widely considered to be among Earth's major 'known unknown' sources of deep carbon into the atmosphere. Our fieldwork coincided with an interval of low-level activity at Bagana and our $CO_2$ emission rates were, accordingly, substantially lower than anticipated (200-320 $td^{-1}$ based on our data, versus a predicted flux of 6200 $td^{-1}$ by Aiuppa et al., 2019). Using multi-year satellite data, we have shown that Bagana's activity, like many volcanoes, is subject to wide temporal variations, and consequently outgassing rates vary widely too. Without any knowledge of the time dependence of plume composition (i.e. $CO_2/SO_2$), we argue that it is incorrect to extrapolate our short campaign data into longer term emissions estimates. In September 2019, Bagana was not likely to be among the major global volcanic carbon emitters. During intervals of elevated unrest, when both $CO_2/SO_2$ ratio and $SO_2$ emissions are likely to be higher than our measurements, we might anticipate $CO_2$ emission rates of $>10^4$ $td^{-1}$. A major challenge for the global volcanological research and monitoring community is how to capture variable gas composition at remote volcanoes or those otherwise without continuous or repeated measurements of gas chemistry. In the immediate term, long-term monitoring of such remote volcanoes as Bagana is to depend heavily on satellite observations, e.g. the $SO_2$ and thermal data we present here, with regular deployments of UAS potentially being made by local and regional observatory staff during periods of heightened unrest and threat.

## Acknowledgments

BMK, EJL and AA acknowledge the financial support of the Alfred P Sloan foundation, awarded via the Deep Carbon Observatory. TR acknowledges funding via the CASCADE programme, EPSRC Programme Grant EP/R009953/1. CIS acknowledges the financial support of the New Zealand Earthquake Commission. The field team (BMK, EJL, KW, TCW, CIS, KM) are grateful to the Bougainville Disaster Office for logistical support and their valuable discussions around hazard and risk mitigation in the region, notably Michaelin Rave and colleagues for assistance in the field. We thank Alphonse and Sylton Vatsi for field support and are deeply grateful to Steven Naget and family, and all the people of Wakovi, for their warm hospitality, their assistance in traversing challenging terrain, and their insights into the historical and modern activity of Bagana. CH & MB acknowledge the UK Natural Environment Research Council funded V-PLUS project (NE/S004106/1). BMK acknowledges the NERC Centre for Observation and Modelling of Earthquakes, Volcanoes and Tectonics (COMET), which supported his first visit to Bagana and laid the groundwork for this study.

## Open Research

Following acceptance/publication, our data will be stored in the Earthchem repository, specifically the DECADe portal which has recently been developed for the archival of volcanic gas data, including time series (https://earthchem.org/ecl/).

## References


Aiuppa, A., Federico, C., Giudice, G., Gurrieri, S. (2005). Chemical mapping of a fumarolic field: La Fossa Crater, Vulcano Island (Aeolian Islands, Italy). Geophysical Research Letters, 32 (13), pp. 1-4.

Aiuppa, A., Moretti, R., Federico, C., Giudice, G., Gurrieri, S., Liuzzo, M., Papale, P., Shinohara, H., Valenza, M. (2007) Forecasting Etna eruptions by real-time observation of volcanic gas composition. Geology, 35 (12), pp. 1115-1118.

Aiuppa, A., Bitetto, M., Francofonte, V., Velasquez, G., Parra, C.B., Giudice, G., Liuzzo, M., Moretti, R., Moussallam, Y., Peters, N., Tamburello, G., Valderrama, O.A., Curtis, A. (2017). A CO2-gas precursor to the March 2015 Villarrica volcano eruption. Geochemistry, Geophysics, Geosystems, 18 (6), pp. 2120-2132.

Aiuppa, A., Fischer, T.P., Plank, T., Bani, P. (2019). CO2 flux emissions from the Earth's most actively degassing volcanoes, 2005–2015. Scientific Reports, 9 (1), art. no. 5442.

Andres, R.J., Kasgnoc, A.D. (1998). A time-averaged inventory of subaerial volcanic sulfur emissions. Journal of Geophysical Research Atmospheres, 103 (D19), art. no. 98JD02091, pp. 25251-25261.

Blake, D.H. (1968). Post miocene volcanoes on Bougainville Island, territory of Papua and New Guinea. Bulletin Volcanologique, 32 (1), pp. 121-138.

Bultitude, R. (1976). Eruptive history of Bagana volcano, Papua New Guinea, between 1882 and 1975, *in* Volcanism in Australasia, ed R. Johnson (Amsterdam: Elsevier), 317–336

Bultitude, R.J. (1981) Literature search for pre-1945 sightings of volcanoes and their activity on Bougainville Island. Cooke-Ravian volume of volcanological papers, pp. 227-242.

Bultitude, R.J., Cooke, R.J.S. (1981) Note on activity from Bagana volcano from 1975 to 1980. Cooke-Ravian volume of volcanological papers, pp. 243-248.

Bultitude, R., Johnson, R., and Chappell, B. (1978). Andesites of Bagana volcano, Papua New Guinea: chemical stratigraphy, and a reference andesite composition. BMR J. Aust. Geol. Geophys. 3, 281–295.

Burton, M., Hayer, C., Miller, C., Christenson, B. (2021). Insights into the 9 December 2019 eruption of Whakaari/White Island from analysis of TROPOMI $SO_2$ imagery. Science Advances, 7 (25), art. no. eabg1218.

Campion, R., Delgado-Granados, H., Mori, T. (2015) Image-based correction of the light dilution effect for SO2 camera measurements, Journal of Volcanology and Geothermal Research, 300, pp48-57.

Carn, S.A., Fioletov, V.E., Mclinden, C.A., Li, C., Krotkov, N.A. (2017). A decade of global volcanic SO2 emissions measured from space. Scientific Reports, 7, art. no. 44095.

Coppola, D., Laiolo, M., Cigolini, C., Delle Donne, D., Ripepe, M. (2016). Enhanced volcanic hot-spot detection using MODIS IR data: Results from the MIROVA system. Geological Society Special Publication, 426 (1), pp. 181-205.

Coppola, D., Laiolo, M., Cigolini, C., Massimetti, F., Delle Donne, D., Ripepe, M., Arias, H., Barsotti, S., Parra, C.B., Centeno, R.G., Cevuard, S., Chigna, G., Chun, C., Garaebiti, E., Gonzales, D., Griswold, J., Juarez, J., Lara, L.E., López, C.M., Macedo, O., Mahinda, C., Ogburn, S., Prambada, O., Ramon, P., Ramos, D., Peltier, A., Saunders, S., de Zeeuw-van Dalfsen, E., Varley, N., William, R. (2020). Thermal Remote Sensing for Global Volcano Monitoring: Experiences From the MIROVA System. Frontiers in Earth Science, 7, art. no. 362.

Crook, K.A.W. (1987). Petrology and mineral chemistry of sedimentary rocks from the Western Solomon Sea, Geo-Marine Letters, 6 (4), pp. 203-209.

D'Aleo R, McCormick B, Salem L, Edmonds M, Bitetto M, Tamburello G, Fischer T, Barry P, Galle B, Arellano S, Mulina K, Itikarai I, Wallius J, Aiuppa A. 2017. Preliminary results of a multi-parametric characterisation of gas manifestations from volcanoes in west Papua New Guinea. *Conferenza Rittmann Giovani Ricercatori, 2017.*

de Moor, J.M., Aiuppa, A., Avard, G., Wehrmann, H., Dunbar, N., Muller, C., Tamburello, G., Giudice, G., Liuzzo, M., Moretti, R., Conde, V., Galle, B. (2016). Turmoil at Turrialba Volcano (Costa Rica): Degassing and eruptive processes inferred from high-frequency gas monitoring. Journal of Geophysical Research: Solid Earth, 121 (8), pp. 5761-5775.

de Moor, J.M., Kern, C., Avard, G., Muller, C., Aiuppa, A., Saballos, A., Ibarra, M., LaFemina, P., Protti, M., Fischer, T.P. (2017). A New Sulfur and Carbon Degassing Inventory for the Southern Central American Volcanic Arc: The Importance of Accurate Time-Series Data Sets and Possible Tectonic Processes Responsible for Temporal Variations in Arc-Scale Volatile Emissions. Geochemistry, Geophysics, Geosystems, 18 (12), pp. 4437-4468.

Draxler, R.R., and G.D. Hess, 1998: An overview of the HYSPLIT_4 modeling system of trajectories, dispersion, and deposition. Aust. Meteor. Mag., 47, 295-308.

Edmonds, M. (2021). Geochemical monitoring of volcanoes and the mitigation of volcanic gas hazards. In: Forecasting and Planning for Volcanic Hazards, Risks, and Disasters (ed. Papale, P.), Elsevier.

Edmonds, M., Liu, E.J., Cashman, K.V. (2022). Open-vent volcanoes fuelled by depth-integrated magma degassing. Bulletin of Volcanology, 84 (3), art. no. 28.

Fischer, T.P., Arellano, S., Carn, S., Aiuppa, A., Galle, B., Allard, P., Lopez, T., Shinohara, H., Kelly, P., Werner, C., Cardellini, C., Chiodini, G. (2019). The emissions of CO2 and other volatiles from the world's subaerial volcanoes. Scientific Reports, 9 (1), art. no. 18716.

Fischer, T.P. & T.M. Lopez. (2016). First airborne samples of a volcanic plume for δ13C of CO2 determinations. Geophysical Research Letters, 43 (7).

Galle, B., Oppenheimer, C., Geyer, A., McGonigle, A.J.S., Edmonds, M., Horrocks, L. (2003). A miniaturised ultraviolet spectrometer for remote sensing of SO2 fluxes: A new tool for volcano surveillance. Journal of Volcanology and Geothermal Research, 119 (1-4), pp. 241-254.

Gliß, J., Stebel, K., Kylling, A., Dinger, A.S., Sihler, H., Sudbø, A. (2017). Pyplis—a python software toolbox for the analysis of SO2 camera images for emission rate retrievals from point sources. Geosciences (Switzerland), 7 (4), art. no. 134.

Global Volcanism Program, 1983. Report on Bagana (Papua New Guinea) (McClelland, L., ed.). Scientific Event Alert Network Bulletin, 8:9. Smithsonian Institution. https://doi.org/10.5479/si.GVP.SEAN198309-255020.
Global Volcanism Program, 1989. Report on Bagana (Papua New Guinea) (McClelland, L., ed.). Scientific Event Alert Network Bulletin, 14:7. Smithsonian Institution. https://doi.org/10.5479/si.GVP.SEAN198907-255020.
Global Volcanism Program, 2019a. Report on Bagana (Papua New Guinea) (Venzke, E., ed.). Bulletin of the Global Volcanism Network, 50:1. Smithsonian Institution. https://doi.org/10.5479/si.GVP.BGVN201902-255020

Global Volcanism Program, 2019b. Report on Bagana (Papua New Guinea) (Crafford, A.E., and Venzke, E., eds.). Bulletin of the Global Volcanism Network, 44:6. Smithsonian Institution. https://doi.org/10.5479/si.GVP.BGVN201906-25502

Global Volcanism Program, 2019c. Report on Bagana (Papua New Guinea) (Bennis, K.L., and Venzke, E., eds.). Bulletin of the Global Volcanism Network, 44:12. Smithsonian Institution. https://doi.org/10.5479/si.GVP.BGVN201912-255020

Global Volcanism Program, 2020. Report on Bagana (Papua New Guinea) (Venzke, E., ed.). Bulletin of the Global Volcanism Network, 45:7. Smithsonian Institution. https://doi.org/10.5479/si.GVP.BGVN202007-255020

Global Volcanism Program, 2021a. Report on Bagana (Papua New Guinea) (Bennis, K.L., and Venzke, E., eds.). Bulletin of the Global Volcanism Network, 46:1. Smithsonian Institution. https://doi.org/10.5479/si.GVP.BGVN202101-255020

Global Volcanism Program, 2021b. Report on Bagana (Papua New Guinea) (Bennis, K.L., and Venzke, E., eds.). Bulletin of the Global Volcanism Network, 46:9. Smithsonian Institution.

Hergt J, Woodhead J, Johnson RW. 2018. Potassium enrichment in arc lavas: a case study from Bougainville Island. *State of the Arc conference 2018.*

Holm, R.J., Rosenbaum, G., Richards, S.W. (2016). Post 8 Ma reconstruction of Papua New Guinea and Solomon Islands: Microplate tectonics in a convergent plate boundary setting. Earth-

Science Reviews, 156, pp. 66-81.

James, M.R., Carr, B.B., D'Arcy, F., Diefenbach, A.K., Dietterich, H.R., Fornaciai, A., Lev, E., Liu, E.J., Pieri, D.C., Rodgers, M., Smets, B., Terada, A., von Aulock, F.W., Walter, T.R., Wood, K.T., Zorn, E.U.
(2020). Volcanological applications of unoccupied aircraft systems (UAS): Developments, strategies, and future challenges. Volcanica, 3 (1), pp. 64-114.

Kantzas, E.P., McGonigle, A.J.S., Tamburello, G., Aiuppa, A., Bryant, R.G. (2010). Protocols for UV camera volcanic SO2 measurements. Journal of Volcanology and Geothermal Research, 194 (1-3), pp. 55-60.

Kazahaya, K., Shinohara, H., Uto, K., Odai, M., Nakahori, Y., Mori, H., Iino, H., Miyashita, M., Hirabayashi, J. (2004). Gigantic SO2 emission from Miyakejima volcano, Japan, caused by caldera collapse. Geology, 32 (5), pp. 425-428.

Kazahaya, R., Shinohara, H., Ohminato, T., Kaneko, T. (2019). Airborne measurements of volcanic gas composition during unrest at Kuchinoerabujima volcano, Japan. Bulletin of Volcanology, 81 (2), art. no. 7.

Kern, C., Lerner, A.H., Elias, T., Nadeau, P.A., Holland, L., Kelly, P.J., Werner, C.A., Clor, L.E., Cappos, M. (2020). Quantifying gas emissions associated with the 2018 rift eruption of Kīlauea Volcano using ground-based DOAS measurements. Bulletin of Volcanology, 82 (7), art. no. 55.

Kern, C., Aiuppa, A., de Moor, J.M. (2022). A golden era for volcanic gas geochemistry? Bulletin of Volcanology, 84 (5), art. no. 43.

Kern, C., Deutschmann, T., Werner, C., Sutton, A.J., Elias, T., Kelly, P.J. (2012). Improving the accuracy of SO2 column densities and emission rates obtained from upward-looking UV-spectroscopic measurements of volcanic plumes by taking realistic radiative transfer into account. Journal of Geophysical Research Atmospheres, 117 (20), art. no. D20302.

Liu, E.J., Wood, K., Mason, E., Edmonds, M., Aiuppa, A., Giudice, G., Bitetto, M., Francofonte, V., Burrow, S., Richardson, T., Watson, M., Pering, T.D., Wilkes, T.C., McGonigle, A.J.S., Velasquez, G., Melgarejo, C., Bucarey, C. (2019). Dynamics of Outgassing and Plume Transport Revealed by Proximal Unmanned Aerial System (UAS) Measurements at Volcán Villarrica, Chile. Geochemistry, Geophysics, Geosystems, 20 (2), pp. 730-750.

Liu, E.J., Aiuppa, A., Alan, A., Arellano, S., Bitetto, M., Bobrowski, N., Carn, S., Clarke, R., Corrales, E., De Moor, J.M., Diaz, J.A., Edmonds, M., Fischer, T.P., Freer, J., Fricke, G.M., Galle, B., Gerdes, G., Giudice, G., Gutmann, A., Hayer, C., Itikarai, I., Jones, J., Mason, E., McCormick Kilbride, B.T., Mulina, K., Nowicki, S., Rahilly, K., Richardson, T., Rüdiger, J., Schipper, C.I., Watson, I.M., Wood, K. (2020).
Aerial strategies advance volcanic gas measurements at inaccessible, strongly degassing volcanoes

(2020a) Science Advances, 6 (44), art. no. abb9103.

Liu, E.J., Cashman, K.V., Miller, E., Moore, H., Edmonds, M., Kunz, B.E., Jenner, F., Chigna, G. (2020b).
Petrologic monitoring at Volcán de Fuego, Guatemala. Journal of Volcanology and Geothermal Research, 405, art. no. 107044.

Massimetti F, Coppola D, Laiola M, Valade S, Cigolini C, Ripepe M, (2020). Volcanic Hot-Spot detection using SENTINEL-2: A comparison with MODIS-MIROVA thermal data series. Remote Sensing, 12 (5).

Mather, T.A., Pyle, D.M., Tsanev, V.I., McGonigle, A.J.S., Oppenheimer, C., Allen, A.G. (2006). A reassessment of current volcanic emissions from the Central American arc with specific examples from Nicaragua. Journal of Volcanology and Geothermal Research, 149 (3-4), pp. 297-311.

McCormick, B., Popp, C., Andrews, B., Cottrell, E. (2015). Ten years of satellite observations reveal highly variable sulphur dioxide emissions at Anatahan Volcano, Mariana Islands. Journal of Geophysical Research, 120 (14), pp. 7258-7282.

McCormick, B.T., Edmonds, M., Mather, T.A., Carn, S.A. (2012). First synoptic analysis of volcanic degassing in Papua New Guinea. Geochemistry, Geophysics, Geosystems, 13 (3), art. no. 7.

McCormick Kilbride, B.T., Mulina, K., Wadge, G., Johnson, R.W., Itikarai, I., Edmonds, M. (2019).
Multi-year satellite observations of sulfur dioxide gas emissions and lava extrusion at Bagana volcano, Papua New Guinea, Frontiers in Earth Science, 7, art. no. 9.
McGonigle, A.J.S., Oppenheimer, C., Tsanev, V.I., Saunders, S., Mulina, K., Tohui, S., Bosco, J., Nahou, J., Kuduon, J., Taranu, F. (2004). Sulphur dioxide fluxes from Papua New Guinea's volcanoes. Geophysical Research Letters, 31 (8), pp. L08606 1-4.

McGonigle, A.J.S., Aiuppa, A., Giudice, G., Tamburello, G., Hodson, A.J., Gurrieri, S. (2008). Unmanned aerial vehicle measurements of volcanic carbon dioxide fluxes. Geophysical Research Letters, 35 (6), art. no. L06303.

Mori, T., Burton, M. (2006). The SO2 camera: A simple, fast and cheap method for ground-based imaging of SO2 in volcanic plumes. Geophysical Research Letters, 33 (24), art. no. L24804.

Mori, T., Shinohara, H., Kazahaya, K., Hirabayashi, J.-I., Matsushima, T., Mori, T., Ohwada, M., Odai, M., Iino, H., Miyashita, M. (2013). Time-averaged SO2 fluxes of subduction-zone volcanoes: Example of a 32-year exhaustive survey for Japanese volcanoes. Journal of Geophysical Research Atmospheres, 118 (15), pp. 8662-8674.

1259 Pering, T.D., Liu, E.J., Wood, K., Wilkes, T.C., Aiuppa, A., Tamburello, G., Bitetto, M.,
1260 Richardson, T., McGonigle, A.J.S. (2020). Combined ground and aerial measurements resolve
1261 vent-specific gas fluxes from a multi-vent volcano. Nature Communications, 11 (1), art. no.
1262 3039.
1263
1264 Queißer, M., Burton, M., Theys, N., Pardini, F., Salerno, G., Caltabiano, T., Varnam, M., Esse,
1265 B., Kazahaya, R. (2019). TROPOMI enables high resolution SO2 flux observations from Mt.
1266 Etna, Italy, and beyond. Scientific Reports, 9 (1), art. no. 957.
1267
1268 Roberge, J., Delgado-Granados, H., Wallace, P.J. (2009). Mafic magma recharge supplies high
1269 CO2 and So2 gas fluxes from Popocatépetl volcano, Mexico. Geology, 37 (2), pp. 107-110.
1270
1271 Rüdiger, J., Tirpitz, J.-L., Maarten De Moor, J., Bobrowski, N., Gutmann, A., Liuzzo, M., Ibarra,
1272 M., Hoffmann, T. (2018). Implementation of electrochemical, optical and denuder-based sensors
1273 and sampling techniques on UAV for volcanic gas measurements: Examples from Masaya,
1274 Turrialba and Stromboli volcanoes. Atmospheric Measurement Techniques, 11 (4), pp. 2441-
1275 2457.
1276
1277 Schellenberg, B., Richardson, T., Watson, M., Greatwood, C., Clarke, R., Thomas, R., Wood, K.,
1278 Freer, J., Thomas, H., Liu, E., Salama, F., Chigna, G. (2019). Remote sensing and identification
1279 of volcanic plumes using fixed-wing UAVs over Volcán de Fuego, Guatemala. Journal of Field
1280 Robotics, 36 (7), pp. 1192-1211.
1281
1282 Shinohara, H., Kazahaya, R., Ohminato, T., Kaneko, T., Tsunogai, U., Morita, M. (2020).
1283 Variation of volcanic gas composition at a poorly accessible volcano: Sakurajima, Japan. Journal
1284 of Volcanology and Geothermal Research, 407, art. no. 107098.
1285
1286 Stix, J., de Moor, J.M., Rüdiger, J., Alan, A., Corrales, E., D'Arcy, F., Diaz, J.A., Liotta, M.
1287 (2018).
1288 Using Drones and Miniaturized Instrumentation to Study Degassing at Turrialba and Masaya
1289 Volcanoes, Central America. Journal of Geophysical Research: Solid Earth, 123 (8), pp. 6501-
1290 6520.
1291
1292 Symonds, R.B., Gerlach, T.M., Reed, M.H. (2001). Magmatic gas scrubbing: Implications for
1293 volcano monitoring. Journal of Volcanology and Geothermal Research, 108 (1-4), pp. 303-341.
1294
1295 Tamburello, G. (2015). Ratiocalc: Software for processing data from multicomponent volcanic
1296 gas analyzers. Computers and Geosciences, 82, pp. 63-67.
1297
1298 Theys, N., Hedelt, P., De Smedt, I., Lerot, C., Yu, H., Vlietinck, J., Pedergnana, M., Arellano, S.,
1299 Galle, B., Fernandez, D., Carlito, C.J.M., Barrington, C., Taisne, B., Delgado-Granados, H.,
1300 Loyola, D., Van Roozendael, M. (2019). Global monitoring of volcanic $SO_2$ degassing with
1301 unprecedented resolution from TROPOMI onboard Sentinel-5 Precursor.Scientific Reports, 9
1302 (1), art. no. 2643.
1303
1304

Theys, N., Fioletov, V., Li, C., De Smedt, I., Lerot, C., McLinden, C., Krotkov, N., Griffin, D., Clarisse, L., Hedelt, P., Loyola, D., Wagner, T., Kumar, V., Innes, A., Ribas, R., Hendrick, F., Vlietinck, J., Brenot, H., Van Roozendael, M. (2021). A sulfur dioxide Covariance-Based Retrieval Algorithm (COBRA): application to TROPOMI reveals new emission sources. Atmospheric Chemistry & Physics, 21, pp. 16727–16744, https://doi.org/10.5194/acp-21-16727-2021.

Veefkind, J.P., Aben, I., McMullan, K., Förster, H., de Vries, J., Otter, G., Claas, J., Eskes, H.J., de Haan, J.F., Kleipool, Q., van Weele, M., Hasekamp, O., Hoogeveen, R., Landgraf, J., Snel, R., Tol, P., Ingmann, P., Voors, R., Kruizinga, B., Vink, R., Visser, H., Levelt, P.F. (2012). TROPOMI on the ESA Sentinel-5 Precursor: A GMES mission for global observations of the atmospheric composition for climate, air quality and ozone layer applications. Remote Sensing of Environment, 120, pp. 70-83.

Wadge, G., Saunders, S., Itikarai, I. (2012). Pulsatory andesite lava flow at Bagana Volcano. Geochemistry, Geophysics, Geosystems, 13 (11), art. no. Q11011.

Wadge, G., McCormick Kilbride, B.T., Edmonds, M., Johnson, R.W. (2018). Persistent growth of a young andesite lava cone: Bagana volcano, Papua New Guinea. Journal of Volcanology and Geothermal Research, 356, pp. 304-315.

Werner C, Kelly PJ, Doukas M, Lopez T, Pfeffer M, McGimsey R, Neal C. (2013). Degassing of CO2, SO2, and H2S associated with the 2009 eruption of Redoubt Volcano, Alaska. Journal of Volcanology and Geothermal Research, 259.

Werner C, Fischer T, Aiuppa A., Edmonds M, Cardellini C, Carn S, Chiodini G, Cottrell E, Burton M, Shinohara H, Allard P. 2019. Carbon dioxide emissions from subaerial volcanic regions: two decades in review. *In:* Deep Carbon: Past to Present (ed. Orcutt B, Daniel I, Dasgupta R), Cambridge University Press.

Wilkes, T.C., McGonigle, A.J.S., Pering, T.D., Taggart, A.J., White, B.S., Bryant, R.G., Willmott, J.R. (2016). Ultraviolet imaging with low cost smartphone sensors: Development and application of a raspberry pi-based UV camera. Sensors (Switzerland), 16 (10), art. no. 1649.

Wilkes, T.C., Pering, T.D., McGonigle, A.J.S., Tamburello, G., Willmott, J.R. (2017). A low-cost smartphone sensor-based UV camera for volcanic SO2 emission measurements. Remote Sensing, 9 (1), art. no. 27.

Wood, K., et al. (2019). A deconvolution-based sensor response correction for volcanic gas measurements, Poster F41, Deep Carbon 2019, Washington, D.C.

Wood, K., Liu, E.J., Richardson, T., Clarke, R., Freer, J., Aiuppa, A., Giudice, G., Bitetto, M., Mulina, K., Itikarai, I. (2020). BVLOS UAS Operations in Highly-Turbulent Volcanic Plumes. Frontiers in Robotics and AI, 7, art. no. 549716.

1350 Woodhead, J.D., Eggins, S.M., Johnson, R.W. (1998). Magma genesis in the New Britain island
1351 arc: further insights into melting and mass transfer processes. Journal of Petrology, 39 (9), pp.
1352 1641-1668.
1353
1354
1355